

# THE SANDSTONE COMPLEX IN THE BRAZOS RIVERBED SECTION: GEOCHEMICAL CONSTRAINTS ON GENESIS AND DEPOSITIONAL CONDITIONS

DIRK MUNSEL, ZSOLT BERNER, AND DORIS STÜBEN  
*Karlsruher Institut für Technologie, 76131 Karlsruhe, Germany*  
*e-mail: zsolt-attila.berner@kit.edu*

**ABSTRACT:** The origin and deposition of spherule-bearing, dominantly sandy beds in a sandstone complex (also called “event deposit”) below the biostratigraphic Cretaceous–Tertiary (KT) boundary plays a key role in models linking the KT mass extinction to the Chicxulub impact. This study, which focuses on the chemostratigraphy of this complex exposed in a ca. 60-cm-thick succession along the Brazos River, Falls County, Texas, U.S.A., aims to constrain the source of the material as well as the depositional conditions and postdepositional history of this highly controversial stratigraphic unit. Major and trace elements, as well as the isotopic composition of the Ca carbonate, contrast sharply with the underlying Corsicana Formation, indicating a dramatic change in the source of material and depositional conditions. Evaluation of geochemical data by principal-component analysis permits identification of (1) siliciclastic components, (2) ejecta material, consisting of altered impact-glass spherules, and (3) Ca carbonate. The ejecta material, originally represented chiefly by glass spherules with carbonate infill, is strongly altered to clay minerals with dominantly smectitic composition and is characterized by the element association  $\text{Al}_2\text{O}_3$ ,  $\text{TiO}_2$ ,  $\text{Fe}_2\text{O}_3$ ,  $\text{P}_2\text{O}_5$ , and  $\text{SO}_2$  and the trace elements (TE) V, Cr, Ni, Cu, Zn, Ga, and Mo. The occurrence of two moderately high Ir peaks (0.2 and 1.1  $\mu\text{g}/\text{kg}$ ) suggests the presence of tiny amounts of extraterrestrial material within the sandstone complex. Based on the contrasting abundance of Ni and Cu in chondritic meteorites and middle crust, the Ni/Cu ratio was used to trace the portion of extraterrestrial material in the sequence. The distribution of this ratio reflects changes in the amount of siliciclastic components added during deposition of the sandstone complex rather than variations in the amount of meteoritic material. The disagreement between evidence suggesting a prevalence of reducing conditions during the alteration of the ejecta material (pyrite inclusions in spherules; accommodation of  $\text{Mn}^{2+}$  by secondary calcite) and sedimentologic features which indicate that the sandstone complex was deposited in a dominantly oxic, high-energy environment strongly supports the case that the ejecta material in these deposits was subjected to reworking.

**KEY WORDS:** KT Brazos, sandstone complex, genesis, depositional constraints

## INTRODUCTION

Numerous studies have investigated the Cretaceous (K)–Palaeocene (T) transition around the Gulf of Mexico and adjacent areas, including Texas (e.g., Smit, 1999; Keller et al., 2003; Keller et al., 2007; Schulte et al., 2003; Schulte et al., 2006). Most intriguing in these KT sequences is the presence of a graded, mostly coarse-grained sandstone complex. In Texas, where the most complete and best exposed KT sections occur along the Brazos River, Falls County, this sandstone complex is often referred to as “event deposit” or “boundary (event) complex” (e.g., Bourgeois et al., 1988; Yancey, 1996; Heymann et al., 1998).

The origin of the sandstone complex has been controversial for more than two decades. The presence of spherules and occasional increased Ir contents has led to a wide acceptance of the idea that the deposition of the sandstone complex is linked in some way to an impact event. It has been postulated that the whole sandstone complex was deposited within a very short time by mega-tsunami waves generated by the Chicxulub impact on Yucatán, which was also believed to have caused the KT mass extinction (e.g., Bourgeois et al., 1988; Smit et al., 1992; Smit et al., 1996; Heymann et al., 1998; Smit, 1999; Arenillas et al., 2006; Schulte et al., 2006). In this scenario, the thin limestone and mudstone layers between the sandstone complex and the KT boundary are interpreted as having settled out from the weak waves after the mega-tsunami subsided. However, a series of sedimentary features within the sandstone complex in Texas and Mexico could not be reconciled with this scenario. For example, the presence of burrows in discrete layers of the sandstone complex, lithoclasts containing spherules, multiple spherule layers (some separated by limestone), and erosional surfaces all indicate that the sequence was deposited during a considerable time interval (Adatte et al., 1996; Keller et al.,

1997; Keller et al., 2003; Keller et al., 2007; Keller et al., 2009; Keller et al., 2010; Gale, 2006). In light of this evidence, the very popular impact scenario has been challenged by a series of papers in which the sandstone complex in northeastern Mexico has been interpreted to represent a sea-level fall with evidence of sediment filling in submarine channels carved along the continental slope (Stinnesbeck et al., 1993; Adatte et al., 1996; Ekdale and Stinnesbeck, 1998; Keller et al., 2003; Keller et al., 2007). Similarly, the sandstone complex in the shallow inner-shelf sections in Brazos, Texas, has been interpreted as lowstand incised-channel fillings, debris flows, or a series of storm deposits emplaced during sea-level lows and following early transgressions during the Late Cretaceous (e.g., Hansen et al., 1987; Yancey, 1996; Gale, 2006; Keller et al., 2007). According to this interpretation, the impact markers represent reworked material from earlier-deposited sediments (e.g., lithified clasts with impact spherules; discussed in Keller et al., 2007).

This study concentrates on the geochemical features of the various subdivisions of the sandstone complex as it appears in a classical section exposed in the Brazos River bed. By applying a variety of geochemical methods in combination with a multivariate statistical approach, we aim to gain new insights into the depositional conditions and postdepositional history of this critical and highly controversial sedimentary complex.

## LOCATION AND LITHOLOGICAL UNITS

The section investigated in this study is situated ca. 500 m downstream from the Texas Highway 413 Bridge across the Brazos River; throughout the ca. 3-km-long, south-trending outcrop belt (Yancey, 1996) the sandstone complex is exposed repeatedly due to faulting. In February 2007, low water levels allowed a systematic

sampling of the lithological units of the sandstone complex on the west bank of the river.

Lithological subdivisions of the sandstone complex in the Brazos River area follows the nomenclature proposed by Yancey (1996) (Fig. 1). The base of the sampled sequence is composed of weakly bedded, dark gray mudstones with dispersed shell fragments, which form the terminal bed of the Corsicana Formation (samples 1 and 2). Deposited above a scoured surface, the lithological units of the sandstone complex begin with a thin layer (ca. 5 cm) of basal conglomerate (sample 3), composed of clasts of mudstone embedded in a matrix of shell hash (BCB of Yancey, 1996). The base of the overlying spherulitic conglomerate unit (referred to hereafter as SCB) is composed of green to brown, loosely cemented sandstones (samples 4 and 6) with a ca. 2-cm-thick intercalation of shell hash (sample 5). Above it, the sandstones become more compact and form two resistant, gray to light gray spherule-bearing layers (samples 7, 8). The overlying sandstones (samples 9 and 11) are barren of spherules and include a thin glauconitic clay layer (sample 10) (GSB of Yancey, 1996). At closer inspection, most of the rounded, spherule-like grains in this sample correspond to what Yancey and Guillemette (2008) describe as “carbonate accretionary lapillies”. The typical hummocky cross-bedded sandstone unit (referred to hereafter HCS) is split up into a lower and an upper part (samples 12 and 17, respectively) by gray glauconitic sandstones (14 and 16). At the base, the glauconitic sandstones contain two 1-mm-thin red-brown layers (sample 13) and include a shell-hash intercalation (sample 15). The shell hash and the glauconitic sandstone layer immediately above (sample 16) contain abundant tiny spherules. The sequence exposed above the water level ends with marly limestones corresponding to the calcareous clayey bed unit of Yancey (CCH; sample 18). The biostrati-

graphically defined KT boundary which follows up-section was below the water level and could not be sampled.

METHODS

Sampling was carried out perpendicular to bedding, each sample covering the whole interval from the base to the top of a lithologically homogeneous layer. Before sampling, several centimeters of rock was scraped off and removed from each rock layer to ensure that only “fresh” material would be collected. For each sample, a small trench about 5 cm wide and 2 cm deep was carved from each bed, yielding—depending on the thickness of the layer—at least 40 g of sample material. Each sample was divided into two aliquots. One part was homogenized and ground to fine powder with a vibrating agate mill and used for the characterization of the bulk rock material, and the other one was used to pick spherules for a study focused on the geochemistry of the spherules (Ullrich et al., this volume). The main mineral components in the bulk sediment were identified by standard X-ray diffraction technique with a Siemens D500 diffractometer. For determination of trace-element concentrations, an Epsilon 5 (PANalytical, The Netherlands) ED-XRF (energy-dispersive X-ray fluorescence) spectrometer was used. The powdered sample material was placed in cups and covered with a mylar film 6 μm thick. Major elements (ME) were quantified with an S4 Explorer WD-XRF (wavelength-dispersive X-ray fluorescence) spectrometer (Bruker AXS, Germany) on fused glass discs prepared by mixing the powdered sample with SPECTROflux (Alfa Aesar) in a ratio of 1:10. Accuracy and precision were assessed by repeated measurements of certified reference materials (AGV-1, SOIL-VII, SL-1, GXR-1, GXR-2, and

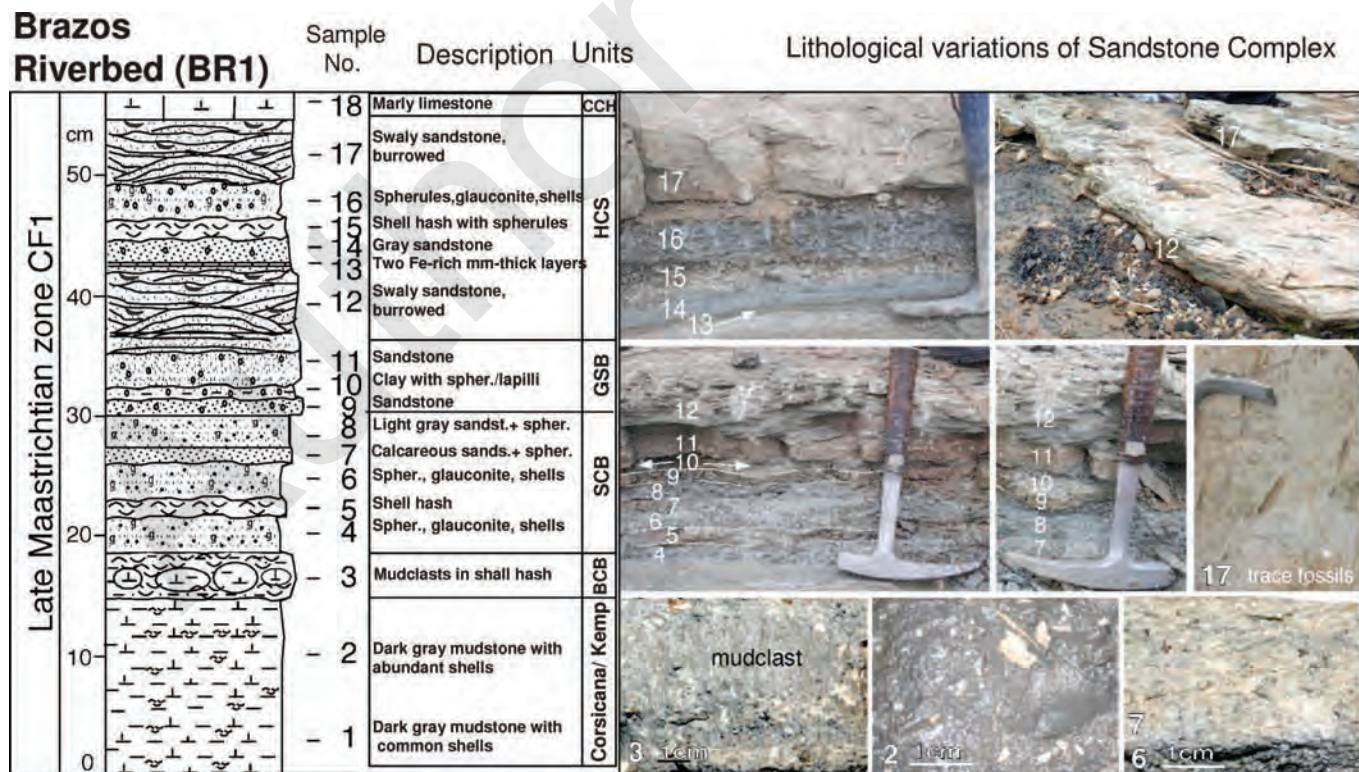


FIGURE 1.—Lithology and position of the samples in the Brazos Riverbed section (after G. Keller).

GXR-3 for ED-XRF; AGV-1, BE-N, and GXR-2 for WD-XRF). Precision was found to be generally better than 5% and 2% for ED-XRF and WD-XRF, respectively. Detection limits for most of the trace elements (TE) are in the range of 3–5 mg/kg. The platinum-group-element (PGE) concentrations were determined by isotope dilution, using pre-concentration and matrix elimination with Ni-fire assay, followed by detection with high resolution ICP-MS (Axiom, VG). The analytical procedure is given in detail in Gertsch et al. (this volume).

Total S and C contents were quantified by a carbon-sulfur analyzer CSA 5003 (Leybold Heraeus) based on nondispersive infrared spectrometric detection. The amounts of both inorganic and carbonate carbon were determined with a carbon-water-analyzer (CWA 5003, Leybold Heraeus). The fraction of organic carbon was assessed by calculating the difference between total carbon and inorganic carbon. Detection limits for both C and S are at 100 ppm.

The isotopic composition of C and O in the carbonate fraction of the sediment was measured with a Delta Advantage IRMS (Thermo Finnigan) coupled on-line with a Gasbach II device for automated carbonate analysis. Each sample run consisted of the measurement of five distinct pulses generated by a reference gas, followed by recording the signals from ten aliquots of CO<sub>2</sub> produced by reaction of the sample with phosphoric acid. Internal precision, based on the standard deviation of the ten peaks, is typically < 0.05‰ for δ<sup>13</sup>C and < 0.08‰ for δ<sup>18</sup>O. Raw data were calibrated versus the V-PDB scale, by measuring the calcite reference material NBS-19 three times after every ten samples. The δ<sup>13</sup>C value of the organic carbon in bulk sediment was determined with an Isoprime IRMS (GV Instrument, UK) coupled on-line to an element analyzer (Euro EA). Prior to analysis, the samples were decarbonated with diluted HCl. Measurements were calibrated versus the V-PDB, using the certified reference materials 24-USGS, 18-NBS, and 21-NBS. Reported values are the average of three individual measurements, with a standard deviation < 0.1‰.

## RESULTS

### *Mineral Composition*

The major mineral phases identified by XRD in the bulk samples include calcite, quartz, and clay minerals. In the spherulitic conglomerate unit (SCB) and the greenish-gray, glauconite-bearing sandstone intercalation of the HCS (sample 16) the portion of detrital phases (quartz, albite) is relatively low. These samples are distinguished by higher concentrations of clay minerals. The XRD spectra of ethylene-glycol-treated material indicate, in concert with previously published data (Schulte et al., 2006; Keller et al., 2007), that the majority of clay minerals are represented by smectite and illite in these layers. Occasionally, notably in the Corsicana Formation, minor amounts of illite-smectite mixed-layer minerals, kaolinite, and chlorite could be detected. Pyrite is subordinate, quantitatively, but it is omnipresent along the section, except in the cross-bedded sandstones of the HCS unit. The presence of glauconite, as suggested by the greenish hue of some of the layers, could be not confirmed by XRD, probably due to low abundance.

### *Major Elements*

The major-element composition of the individual layers of the sandstone complex closely reflects the large range of mixing between silica/silicate and carbonate phases of different origins (Table 1; Fig. 2). Compared to the Corsicana Formation the SiO<sub>2</sub> content in the sandstone complex is generally low, but it tends to increase up-section (from 9.75 to 41.55 wt.%), attaining maximum values in the hummocky cross-bedded sandstone unit (up to 56.33 wt.%), similar to those in the Corsicana Formation (53.7–54.8 wt.%). The SiO<sub>2</sub>/Al<sub>2</sub>O<sub>3</sub> ratio (Fig. 3) is considerably less (2.5–3.0) in the lower, spherule

bearing units than in the sandstones of the GSB (4.5–5.6) and HCS (6.7–7.6), which suggests that the excess of SiO<sub>2</sub> is due to a higher portion of detrital minerals. The spherule-rich layers (samples 4, 6, 8, 10, and 16) are consistently higher in SiO<sub>2</sub> and Al<sub>2</sub>O<sub>3</sub>, as well as in TiO<sub>2</sub>, Fe<sub>2</sub>O<sub>3</sub>, MgO, P<sub>2</sub>O<sub>5</sub>, and S relative to the non-spherule-bearing intercalations (samples 3, 5, 7, 9, 11, and 17). This increase is evident in the upper glauconitic layer of the HCS (sample 16), which shows the overall highest contents in the afore mentioned elements (1.16 wt.% TiO<sub>2</sub>, 19.15 wt.% Al<sub>2</sub>O<sub>3</sub>, 8.60 wt.% Fe<sub>2</sub>O<sub>3</sub>, 1.82 wt.% MgO, 2.65 wt.% P<sub>2</sub>O<sub>5</sub>, and 9.72 wt.% SO<sub>2</sub>).

The content of the alkali elements is generally low (mostly in the range 0.1 to 0.2 wt.% K<sub>2</sub>O and Na<sub>2</sub>O, respectively), increasing gradually in the GSB and attaining the highest values in the HCS (up to 2.23 wt.% K<sub>2</sub>O and 0.95 wt.% Na<sub>2</sub>O) (Fig. 2). A distinct feature of the sandstone complex in terms of major-element composition is its strong enrichment in CaO. Most of the CaO is bound in carbonate, showing an overall antagonistic behavior to SiO<sub>2</sub> ( $r = -0.93$ ) and the other elements associated with detrital minerals. CaO contents are highest in the lower part of the sandstone complex and decrease gradually from 44.28 wt.% in BCB (sample 3) to 9.74 wt.% in the glauconite-bearing intercalation of the HCS (sample 16), and increase again abruptly in the upper part of the HCS (29.36 wt.%) and in the marly limestone of the CCH immediately above (41.32 wt.%). The noncarbonate CaO (as estimated from total CaO and total inorganic carbon) shows a behavior similar to that of the silicate-bound elements.

Among the major elements, only Mn correlates positively with Ca, suggesting that most of the Mn is accommodated in the calcite lattice. The abundance of organic carbon decreases gradually from 0.43–0.48 wt.% in BCB to 0.05–0.14 wt.% in the hummocky cross-bedded unit. The two highest C<sub>org</sub> values (2.61 and 0.56 wt.% C) are related to shell-bearing layers. Remarkable is the overall high P and S content of the sandstone complex, with an average of 1.38 wt.% P<sub>2</sub>O<sub>5</sub> and 3.7 wt.% SO<sub>2</sub> in the spherule-bearing layers and of 0.55 wt.% P<sub>2</sub>O<sub>5</sub> and 1.66 wt.% SO<sub>2</sub> in the other samples. Compared to these, the abundance of P<sub>2</sub>O<sub>5</sub> in the Corsicana Formation is 0.23–0.27 wt.%.

### *Trace Elements*

Large ions carrying weak charges (large-ion lithophile elements: LILE) and small ions carrying strong charges (high-field-strength elements: HFSE) are called incompatible because they are accommodated with difficulty by most of the minerals of the mantle and consequently tend to become concentrated in felsic rocks and the continental crust. A prominent feature of the distribution of the trace elements (Table 2) is a strong depletion of the incompatible elements in the sandstone complex relative to the mudstones of the Corsicana Formation. This is most evident for the LILE, which drop from average values of 94.3 mg/kg Rb, 13.5 mg/kg Cs, 337 mg/kg Ba, and 16.4 mg/kg Pb in the Corsicana Formation to averages of 19.6, 9.3, 175, and 4.7 mg/kg, respectively, in the sandstone complex (Table 2). The decrease in the abundance of these elements is even stronger if only the spherule-rich layers are considered (5.8, 8.4, 101, and 3.5 mg/kg for Rb, Cs, Ba and Pb, respectively). A similar change can be observed also in the abundance of strongly immobile HFSE. The Th contents decrease from 9.9 mg/kg in the mudstones of the Corsicana Formation to an average of 5.9 mg/kg in the spherule-bearing layers of the sandstone complex (samples 4, 5, 6, 7, 8, 15 and 16), from 182 to 76.7 mg/kg for Zr, and from 12.4 to 3.3 mg/kg for Nb. For REE (rare earth elements), including Y, the discrepancies are not as pronounced as for the HFSE (e.g., 51.8 to 37.6 mg/kg for Ce and 23.5 to 18.4 for Y). Although these differences may be due in part to dilution with carbonate, this trend can be observed also when CaCO<sub>3</sub>-corrected values are considered. Although the abundance of transition metals (V, Cr, Ni, and Zn) is generally also lower in the sandstone complex, their concentrations in the spherule-rich layers (4, 6, 8, and 16) are

TABLE 1.—Major-element composition [wt.%] of the sampled layers in the sandstone complex (LOI = loss on ignition).

|                                | Br1-1 | Br1-2 | Br1-3 | Br1-4 | Br1-5 | Br1-6 | Br1-7 | Br1-8 | Br1-9 | Br1-10 | Br1-11 | Br1-12 | Br1-13 | Br1-14 | Br1-15 | Br1-16 | Br1-17 | Br1-18 |
|--------------------------------|-------|-------|-------|-------|-------|-------|-------|-------|-------|--------|--------|--------|--------|--------|--------|--------|--------|--------|
| SiO <sub>2</sub>               | 54.81 | 53.69 | 9.75  | 18.75 | 10.42 | 14.36 | 11.70 | 26.22 | 20.20 | 41.55  | 24.91  | 50.57  | 54.95  | 56.33  | 25.03  | 36.69  | 35.57  | 12.51  |
| TiO <sub>2</sub>               | 0.63  | 0.65  | 0.20  | 0.40  | 0.20  | 0.31  | 0.19  | 0.58  | 0.19  | 0.54   | 0.21   | 0.34   | 0.59   | 0.51   | 0.38   | 1.18   | 0.25   | 0.15   |
| Al <sub>2</sub> O <sub>3</sub> | 13.37 | 13.96 | 3.55  | 7.20  | 3.66  | 5.49  | 3.86  | 10.55 | 4.35  | 9.16   | 4.43   | 6.61   | 9.63   | 9.38   | 8.01   | 19.15  | 5.27   | 3.55   |
| Fe <sub>2</sub> O <sub>3</sub> | 4.85  | 5.27  | 2.65  | 4.77  | 2.49  | 4.30  | 1.94  | 3.82  | 2.33  | 5.55   | 2.20   | 2.59   | 4.63   | 3.51   | 2.93   | 8.60   | 2.26   | 1.65   |
| MnO                            | 0.03  | 0.04  | 0.25  | 0.18  | 0.22  | 0.19  | 0.21  | 0.14  | 0.17  | 0.07   | 0.14   | 0.12   | 0.05   | 0.05   | 0.19   | 0.03   | 0.15   | 0.18   |
| MgO                            | 1.97  | 2.14  | 1.51  | 2.00  | 1.63  | 1.87  | 1.44  | 2.32  | 1.54  | 1.83   | 1.27   | 0.95   | 1.58   | 1.55   | 1.75   | 1.82   | 1.04   | 1.17   |
| CaO                            | 8.73  | 6.84  | 44.28 | 32.41 | 43.50 | 37.17 | 43.09 | 28.33 | 37.05 | 17.76  | 34.08  | 18.88  | 9.83   | 11.28  | 32.38  | 9.74   | 29.36  | 41.32  |
| Na <sub>2</sub> O              | 0.87  | 0.74  | 0.13  | 0.15  | 0.09  | 0.10  | 0.11  | 0.22  | 0.38  | 0.61   | 0.43   | 0.92   | 0.74   | 0.95   | 0.25   | 0.33   | 0.79   | 0.17   |
| K <sub>2</sub> O               | 2.23  | 2.10  | 0.25  | 0.15  | 0.12  | 0.11  | 0.16  | 0.23  | 0.56  | 1.05   | 0.71   | 1.28   | 1.13   | 1.34   | 0.41   | 0.44   | 1.08   | 0.51   |
| P <sub>2</sub> O <sub>5</sub>  | 0.23  | 0.27  | 0.48  | 1.44  | 0.63  | 1.17  | 0.44  | 1.39  | 0.61  | 2.70   | 0.49   | 0.31   | 1.84   | 1.01   | 0.64   | 2.65   | 0.14   | 0.09   |
| LOI                            | 12.03 | 13.88 | 35.56 | 30.40 | 35.32 | 33.27 | 35.26 | 24.38 | 31.77 | 17.16  | 30.43  | 17.10  | 11.97  | 13.66  | 27.38  | 16.31  | 23.95  | 36.92  |
| Total                          | 99.75 | 99.58 | 98.61 | 97.85 | 98.28 | 98.34 | 98.40 | 98.18 | 99.15 | 97.98  | 99.30  | 99.67  | 96.94  | 99.57  | 99.35  | 96.94  | 99.86  | 98.22  |
| C <sub>carbonate</sub>         | 1.85  | 1.49  | 9.23  | 6.47  | 8.88  | 5.35  | 8.96  | 5.30  | 7.85  | 3.09   | 7.35   | 3.99   | 1.63   | 2.16   | 6.47   | 1.20   | 6.19   | 9.14   |
| C <sub>organic</sub>           | 0.73  | 0.73  | 0.43  | 0.48  | 0.43  | 2.61  | 0.30  | 0.32  | 0.47  | 0.33   | 0.27   | 0.22   | 0.14   | 0.05   | 0.56   | 0.16   | 0.25   | 0.68   |
| S <sub>total</sub>             | 0.89  | 1.31  | 1.02  | 2.24  | 0.97  | 2.05  | 0.41  | 1.20  | 0.70  | 2.03   | 0.54   | 0.40   | 1.61   | 1.26   | 1.04   | 4.86   | 0.38   | 1.16   |

consistently higher than in those with lower spherule contents (samples 3, 5, 7, 9, and 15). In contrast, Sr as well as a few of the transition and heavy metals (Sc, Cu, Mo, and U) are slightly enriched in the layers of the sandstone complex. The Al-normalized values of some incompatible elements (Rb, Ba, Pb, Zr, and Nb; Fig. 4) also tend to be lower in the spherule-rich lower part of the sandstone complex (BCB and SCB), as compared to the upper part of the complex, which is relatively poor in ejecta material. In contrast, the Al-normalized values of trace elements typically enriched in mafic rocks (such as Sc, V, Ni, and Cu), show the opposite trend (Fig. 4).

*Platinum-Group Elements*

Abundances of platinum-group elements (PGE) were determined in a subset of 11 samples (Table 2). Iridium concentrations well above the analytical background value of 0.2 µg/kg were found only in a thin

clayey layer in GSB (sample 10); however, in this layer the spherical grains correspond more to accretionary carbonate lapilli than to microtektitic spherules (Yancey and Guillemette, 2008). The relatively high Ir content in this sample (1.1 µg/kg) is associated with a slight enrichment also in other PGE (3.2 µg/kg Ru, 3.2 µg/kg Rh, 8.7 µg/kg Pd, and 4.2 µg/kg Pt). Its C1 chondrite-normalized pattern (Fig. 5) shows a slight enrichment of the chalcophiles Rh and Pd relative to the siderophile PGEs (Ir and Ru), which is in concert with the increased pyrite content of this layer. Iridium and Pt concentrations just slightly above the background were also observed in sample 14 (0.2 µg/kg Ir and 1.8 µg/kg Pt).

*Carbon and Oxygen Isotopes*

The isotope composition of carbonate carbon in bulk sediment shows a sharp drop of about 7–8‰ at the transition from the mudstones

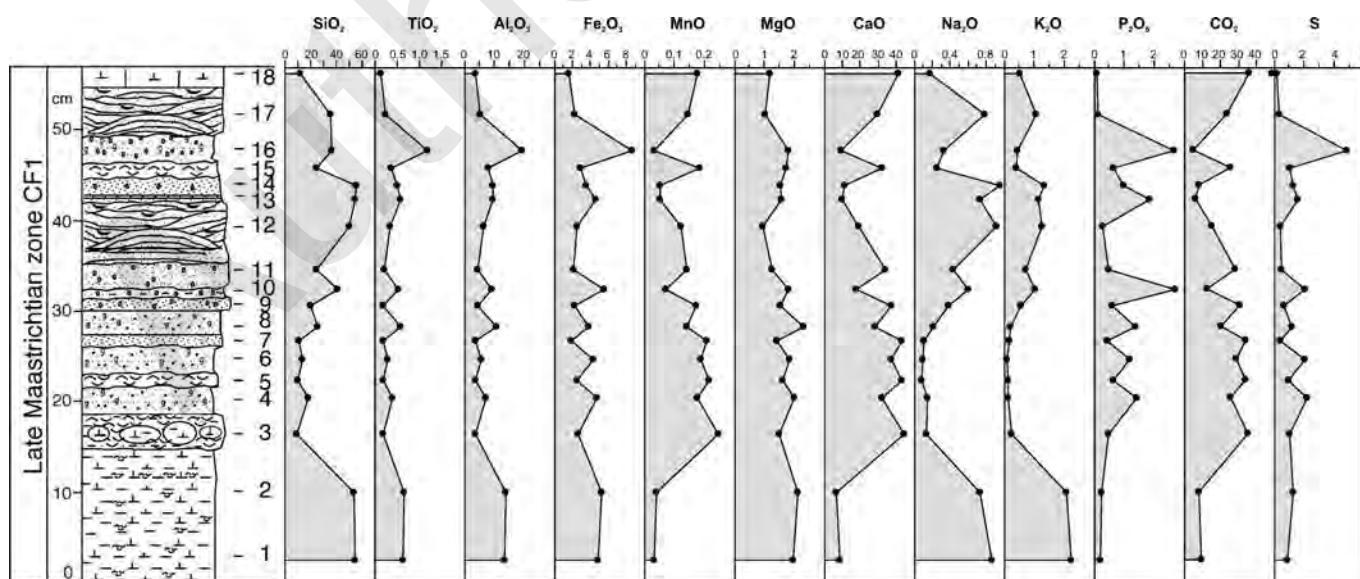


FIGURE 2.—Major-element composition [wt.%] of different lithologies in the Brazos Riverbed section.

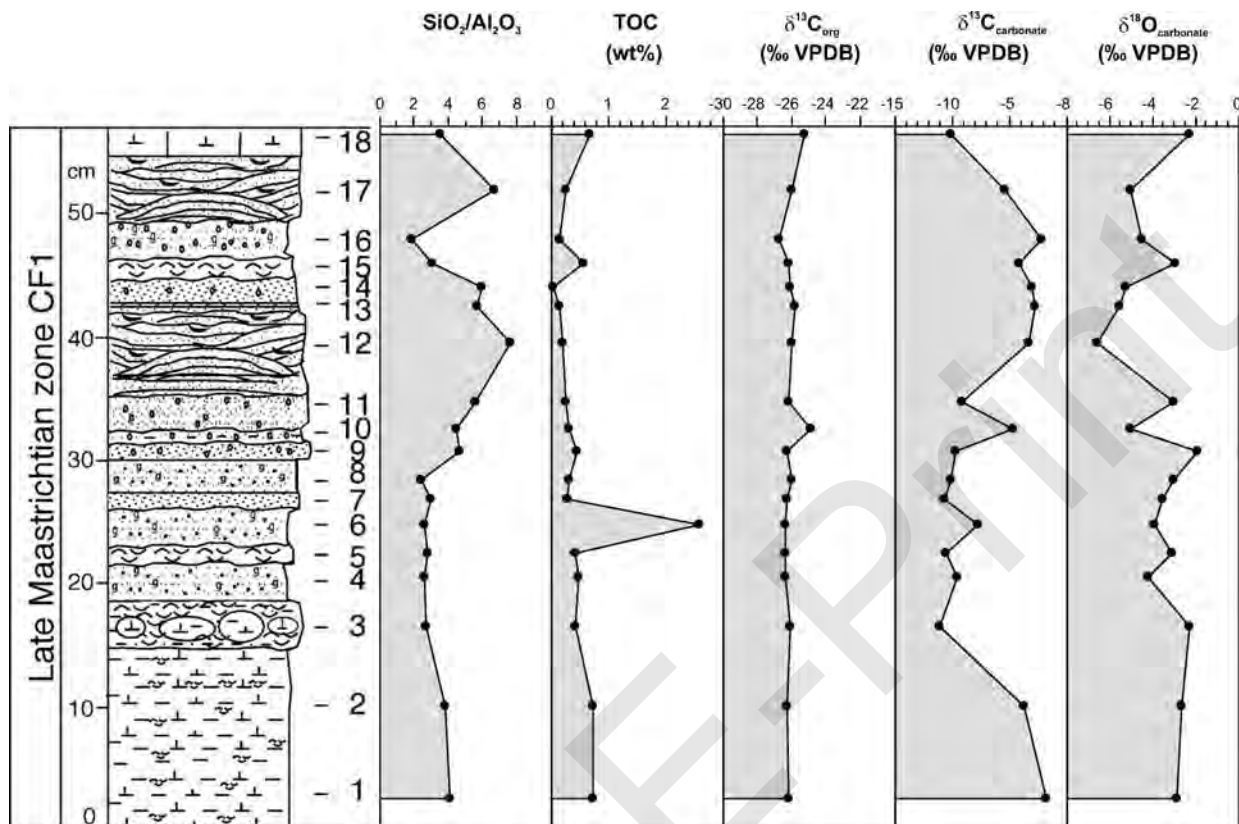


FIGURE 3.—Variation in  $\text{SiO}_2/\text{Al}_2\text{O}_3$  ratio, in total organic carbon (TOC) and in stable-isotope composition of carbonate and organic carbon in lithologies of the Brazos Riverbed section. Please note the increase of the  $\text{SiO}_2/\text{Al}_2\text{O}_3$  ratio toward the top of the section, with the highest values in the hummocky cross-bedded unit (HCS).

of the Corsicana Formation to the sandstone complex (Table 1; Fig. 3). While at the base of the section the  $\delta^{13}\text{C}$  of bulk carbonate ( $-1.74\text{‰}$ ) is within the normal range of Upper Maastrichtian sediments, the first value recorded in the sandstone complex is as low as  $-11.06\text{‰}$ . Except for a short positive excursion in the layer with the carbonate concretionary lapilli (GSB, sample 10;  $\delta^{13}\text{C} = -4.66\text{‰}$ ), low values of around  $-10\text{‰}$  persist within the whole lower portion of the section (BCB, SCB, and GSB). At the boundary between the GSB and the HCS, there is a sudden increase to  $-3.27\text{‰}$ , and a return to very low values ( $-10.05\text{‰}$ ) only in the marly limestones at the top of the section. A striking feature of the sandstone complex is a strong negative correlation between the isotope composition of the carbonate carbon and TIC (total inorganic carbon) content, although the most spherule-rich samples (4, 6, and 8) tend to deviate slightly from the regression line towards even lower  $\delta^{13}\text{C}$  values. There is also a clear difference between the spherule-rich layers of the lower and upper part of the section: the lower units are distinguished by high carbonate content and low  $\delta^{13}\text{C}$  values, while the spherule-bearing intercalations in the cross-bedded sandstones (samples 15 and 16) have lower carbonate contents and are less depleted in  $^{13}\text{C}$ .

The oxygen isotopes show trend opposite to that of the carbon isotopes (Fig. 3), and the differences among the units are less pronounced. Relative to the mudstones of the Corsicana Formation ( $\delta^{18}\text{O} = -2.86$  to  $-2.61\text{‰}$ ), the carbonate of the sandstone complex is generally depleted in  $^{18}\text{O}$ , with the lowest values (as low as  $-6.57\text{‰}$ ) recorded in the hummocky sandstones, returning to values similar as in the Corsicana in the marly limestones of the CCH ( $-2.23\text{‰}$ ). The

isotope composition of the organic carbon varies in a very narrow range between  $-25.80$  and  $-26.73\text{‰}$ , with a single value out of this range in the lapilli-rich horizon (sample 10;  $-24.84\text{‰}$ ).

#### Statistical Data Evaluation

Principal-component analysis (PCA) was carried out, using the software Statistica (V 8.0, StatSoft, Inc.), in order to detect the main factors which account for the variance of the geochemical parameters in the sandstone complex. Inconsistencies, which may occur in compositional data with a constant-sum constraint, were eliminated by converting the major-element data prior to the PCA by a centered logratio transformation (*clr*), following the procedure given in Ohta and Arai (2007). The 35 geochemical parameters considered could be reduced by the PCA to only two factors, which explain 82% of the variance expressed by the initial data matrix (Fig. 6).

The first factor (PC1; 44% of the variance) includes a set of major elements and trace elements (Si, Na, K, Ga, Rb, Y, Zr, Nb, Cs, Ba, La, Ce, Pb, and Th) which are typical of the clastic components of the sediments (quartz, feldspars, clay minerals, accessory heavy minerals). Factor loadings of elements of the carbonate phase (Ca, Mg, and Mn) are relatively high in absolute values, but with negative algebraic sign. Such a relationship is common in marine sediments, where it reflects a general decrease in the amount of biogenic carbonate forming during periods of high clastic input.

The second factor (PC2), which explains 38% of the total variance, is characterized by Al, Ti, Fe, P, and S and some transition metals. The

TABLE 2.—Trace-element [mg/kg], PGE [μg/kg], and isotope data [%] of the sampled layers in the sandstone complex (n.a. = not analyzed).

|  | Br1 -1 | Br1 -2 | Br1 -3 | Br1 -4 | Br1 -5 | Br1 -6 | Br1 -7 | Br1 -8 | Br1 -9 | Br1 -10 | Br1 -11 | Br1 -12 | Br1 -13 | Br1 -14 | Br1 -15 | Br1 -16 | Br1 -17 | Br1 -18 |
|--|--------|--------|--------|--------|--------|--------|--------|--------|--------|---------|---------|---------|---------|---------|---------|---------|---------|---------|
| Sc                                     | 25     | 14     | 28     | 36     | 33     | 39     | 39     | 45     | 22     | 24      | 23      | 16      | 16      | 12      | 34      | 16      | 21      | 28      |
| V                                      | 109    | 111    | 24     | 66     | 40     | 109    | 41     | 102    | 31     | 58      | 29      | 15      | 44      | 59      | 101     | 83      | 15      | 24      |
| Cr                                     | 140    | 133    | 26     | 47     | 26     | 74     | 26     | 70     | 35     | 93      | 45      | 44      | 94      | 84      | 42      | 117     | 36      | 23      |
| Ni                                     | 34     | 37     | 18     | 22     | 23     | 26     | 21     | 28     | 22     | 32      | 24      | 26      | 33      | 30      | 24      | 39      | 25      | 23      |
| Cu                                     | 17     | 16     | 15     | 16     | 14     | 21     | 15     | 23     | 12     | 20      | 13      | 13      | 16      | 15      | 17      | 32      | 15      | 14      |
| Zn                                     | 102    | 105    | 37     | 28     | 26     | 38     | 16     | 32     | 32     | 56      | 37      | 37      | 46      | 45      | 32      | 65      | 38      | 37      |
| Ga                                     | 21     | 23     | 12     | 14     | 12     | 16     | 12     | 17     | 13     | 15      | 14      | 14      | 15      | 18      | 15      | 18      | 14      | 13      |
| Rb                                     | 97     | 92     | 8      | 4      | 3      | 7      | 4      | 6      | 20     | 39      | 26      | 41      | 34      | 40      | 14      | 11      | 34      | 24      |
| Sr                                     | 386    | 345    | 440    | 399    | 349    | 468    | 401    | 421    | 353    | 536     | 337     | 302     | 401     | 367     | 540     | 446     | 399     | 552     |
| Y                                      | 25     | 23     | 19     | 18     | 11     | 23     | 15     | 21     | 22     | 41      | 20      | 21      | 42      | 33      | 15      | 23      | 20      | 11      |
| Zr                                     | 192    | 172    | 39     | 67     | 38     | 87     | 44     | 94     | 87     | 151     | 98      | 303     | 350     | 320     | 91      | 129     | 155     | 42      |
| Nb                                     | 13     | 12     | 1      | 3      | 1      | 3      | 1      | 4      | 2      | 6       | 4       | 7       | 8       | 8       | 4       | 7       | 5       | 3       |
| Mo                                     | 4      | 5      | 18     | 21     | 2      | 8      | 1      | 11     | 3      | 12      | 2       | 5       | 9       | 7       | 4       | 45      | 4       | 0       |
| Cs                                     | 12     | 15     | 9      | 8      | 8      | 8      | 8      | 8      | 9      | 10      | 10      | 10      | 10      | 12      | 8       | 10      | 11      | 10      |
| Ba                                     | 321    | 353    | 77     | 99     | 63     | 106    | 54     | 91     | 120    | 273     | 173     | 328     | 326     | 344     | 117     | 194     | 313     | 126     |
| La                                     | 30     | 28     | 21     | 24     | 19     | 23     | 20     | 23     | 24     | 40      | 26      | 25      | 43      | 35      | 20      | 33      | 24      | 19      |
| Ce                                     | 52     | 52     | 29     | 37     | 25     | 39     | 27     | 37     | 38     | 70      | 42      | 44      | 83      | 66      | 32      | 61      | 42      | 27      |
| Pb                                     | 14     | 19     | 1      | 2      | 2      | 3      | 2      | 5      | 3      | 8       | 5       | 7       | 8       | 6       | 3       | 7       | 11      | 2       |
| Th                                     | 10     | 10     | 6      | 6      | 5      | 6      | 5      | 6      | 7      | 8       | 8       | 7       | 8       | 7       | 6       | 6       | 8       | 7       |
| U                                      | 6      | 4      | 5      | 2      | 4      | 7      | 5      | 3      | 6      | 9       | 9       | 4       | 6       | 6       | 6       | 9       | 4       | 8       |
| Ru                                     | 0.5    | n.a.   | n.a.   | 0.5    | n.a.   | 0.5    | n.a.   | n.a.   | 0.5    | 3.2     | 0.5     | 0.5     | 0.5     | 0.5     | n.a.    | 0.5     | n.a.    | 0.5     |
| Rh                                     | 0.1    | n.a.   | n.a.   | 0.1    | n.a.   | 0.1    | n.a.   | n.a.   | 0.1    | 3.2     | 0.1     | 0.1     | 0.1     | 0.1     | n.a.    | 0.1     | n.a.    | 0.1     |
| Pd                                     | 0.8    | n.a.   | n.a.   | 1.5    | n.a.   | 0.7    | n.a.   | n.a.   | 2.3    | 8.7     | 0.7     | 0.7     | 0.7     | 0.7     | n.a.    | 0.7     | n.a.    | 1.6     |
| Ir                                     | 0.2    | n.a.   | n.a.   | 0.2    | n.a.   | 0.2    | n.a.   | n.a.   | 0.2    | 1.1     | 0.2     | 0.2     | 0.2     | 0.2     | n.a.    | 0.2     | n.a.    | 0.2     |
| Pt                                     | 0.9    | n.a.   | n.a.   | 7.0    | n.a.   | 4.7    | n.a.   | n.a.   | 3.2    | 4.2     | 1.9     | 2.9     | 2.4     | 1.8     | n.a.    | 2.2     | n.a.    | 12.0    |
| δ <sup>13</sup> C <sub>carbonate</sub> | -1.74  | -3.75  | -11.06 | -9.48  | -10.52 | -7.67  | -10.63 | -10.1  | -9.59  | -4.66   | -9.14   | -3.27   | -2.67   | -2.94   | -4.14   | -2.12   | -5.4    | -10.05  |
| δ <sup>18</sup> O <sub>carbonate</sub> | -2.86  | -2.61  | -2.27  | -4.18  | -3.05  | -3.86  | -3.55  | -3.01  | -1.86  | -4.97   | -3.02   | -6.57   | -5.51   | -5.25   | -2.96   | -4.5    | -5.03   | -2.23   |
| δ <sup>13</sup> C <sub>org</sub>       | -26.16 | -26.24 | -26.02 | -26.38 | -26.33 | -26.35 | -26.26 | -25.94 | -26.28 | -24.84  | -26.14  | -25.97  | -25.8   | -26.05  | -26.2   | -26.73  | -25.94  | -25.23  |

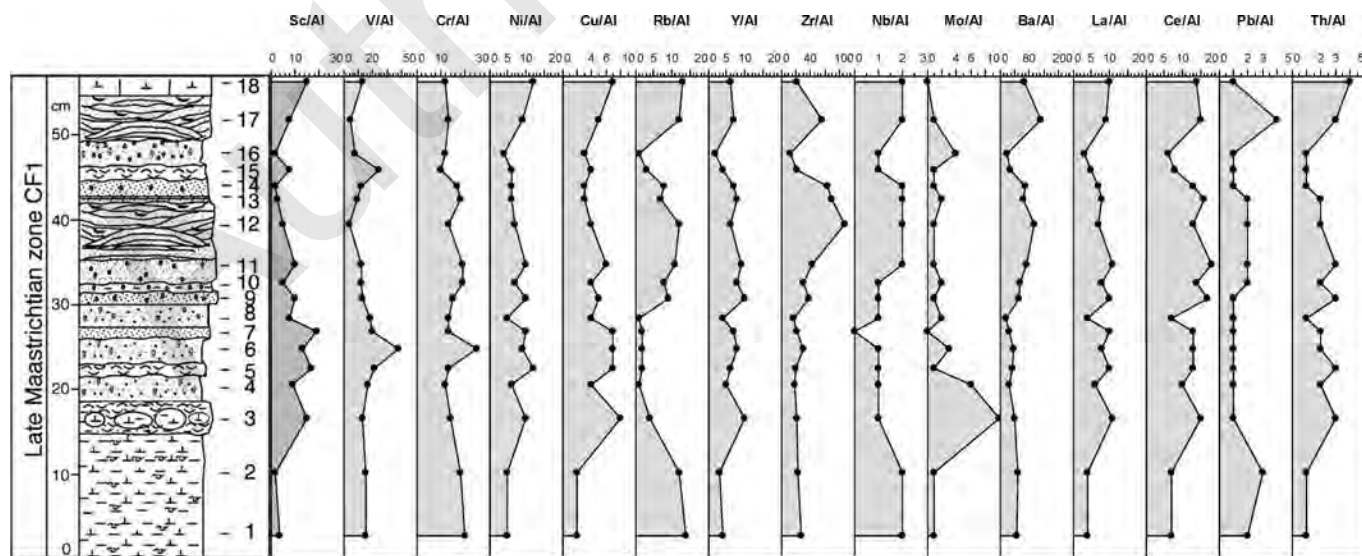


FIGURE 4.—Aluminum-normalized trace-element concentrations in different lithologies of the Brazos Riverbed section.

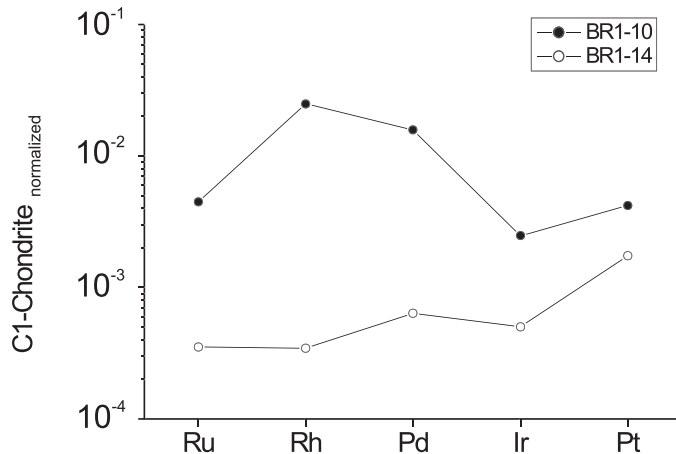


FIGURE 5.—C1-chondrite-normalized PGE concentrations in two samples with slightly increased Ir abundances.

association of Al, Fe, Ti, Ga, V, and Cr suggests a clay-mineral component (smectite, chlorite) that resulted (at least in part) from alteration of a mafic precursor (glass or minerals). On the other hand, the chalcophile elements S, Fe, Cu, Ni, Mo, As, and Zn are more compatible with a sulfidic mineral host (e.g., pyrite). The coincidence of all these elements within the same factor hints of a common origin for both components. Similar to PC1, parameters of the carbonate phase, notably CaO, total inorganic C, LOI (loss on ignition), but also some minor elements, like Mn and Sr, also have opposite algebraic sign relative to the other elements. The loading of  $\delta^{13}\text{C}_{\text{carb}}$  and  $\delta^{18}\text{O}_{\text{carb}}$  are also diametrical, indicating that the carbonate associated with spherules is depleted in  $^{13}\text{C}$  and slightly enriched in  $^{18}\text{O}$ .

The recalculation of the factor scores by an isometric logratio transformation (*ilr*; Ohta and Arai, 2007) enables the representation of the samples in a ternary plot and allows a general characterization of the various lithological units in terms of their mineralogical and geochemical composition (Fig. 7). According to this, the sandstones of the HCS unit (samples 12, 13, 14, and 17) are distinguished by low portions of carbonates and high siliciclastic contents. Although the sediments of the Corsicana Formation have an even higher amount of clastic compounds, this is due primarily to a higher portion of clay minerals (and possibly some feldspars) and to a lesser extent, quartz, as it is in case of the HCS. Compared to HCS, the sandstones of the GSB (samples 9 and 11) have higher amounts of carbonate and lower siliciclastic compounds. The spherule-rich layers of the SCB and the GSB (samples 4, 6, 8, and 16) contain various amounts of a  $^{13}\text{C}$ -depleted carbonate, whereas the marly limestone at the top of the cross-bedded sandstones (sample 18) shows an elemental and isotopic composition roughly similar to that of the mud clasts at the base of the complex.

## DISCUSSION

### Source of Constituents

The sharp switch in the major-element and trace-element compositions of the sediments at the boundary between the Corsicana Formation and the sandstone complex (Table 1 and 2; Figs. 2 and 4) clearly indicates a sudden change in the sediment source. A plot of the sample scores in a diagram defined by the two factor axes reveals considerable differences in the composition of samples taken from different lithologies and allows inferences on the source of the sediment components (Fig. 6). Samples rich in spherules (4, 6, 8, and

16) show the highest scores for PC2 and low scores for PC1, suggesting that factor 2 represents the ejecta material. The mineralogical and chemical composition of the microtektites supports this assumption to a large extent. A detailed study from this section (Ullrich et al., this volume) has shown that the spherules essentially represent glassy microtektites that were altered to different clay minerals depending on the original chemical composition of the glass, and the majority contain a calcitic core. In terms of their  $\text{Al}_2\text{O}_3$ – $\text{MgO}$ – $\text{K}_2\text{O}$  contents, the spherule-rich samples show an intermediate position between the two fundamental types of spherules distinguished by Schulte et al. (2006) in the Brazos River section (Mg-rich smectite and chlorite) (Fig. 8).

The opposite algebraic sign of the loadings of the carbonate-mineral and clay-mineral specific parameters indicates that an inverse relationship exists between the amount of biogenic carbonate and ejecta-rich components present in the sample. On the other hand, the relatively low PC1 scores of the spherule-rich layers show that the input of siliciclastic components (quartz and feldspars:  $\text{SiO}_2$ ,  $\text{K}_2\text{O}$ ,  $\text{Na}_2\text{O}$ , Rb, Cs, Ba, Pb, and Th) and of heavy minerals (La, Ce, Y, Nb, and Zr) was relatively low during their deposition.

Based on the major-element and trace-element spectra of the spherule rich layers, the target material that participated in the formation of the ejecta material most likely consisted of basement rocks; however, the alkali elements typical of more acidic rocks could have been removed due to their higher mobility during alteration. The sequence of impactites recovered by the Yaxcopoil-1 drilling (executed as part of the Chicxulub Scientific Drilling Program) allows a comprehensive survey of the composition of the basement rocks and the overlying sedimentary rock sequence in the target area of the Chicxulub impact (Schmitt et al., 2004; Tuchscherer et al., 2004; Kring et al., 2004; Dressler et al., 2004); however, the geochemical heterogeneity of the ejecta encountered in different locations worldwide complicates an accurate reconstruction of all of the precursor material. In the section studied here, the issue is even more problematic because the ejecta material not only is strongly altered, but also is intimately admixed with detrital components and calcite of different origins. In order to enable a better comparison with other published data, the bulk chemical composition of the samples was recalculated after eliminating both the portion of biogenic calcite and the carbonate associated with the lapilli fraction (assessed on basis of their distinct carbon-isotope compositions). Results shown in form of a ternary plot for  $\text{K}_2\text{O}+\text{Na}_2\text{O}-\text{CaO}-\text{MgO}+\text{FeO}_{\text{tot}}$  (Fig. 9) are compared with the sequence of impactites recovered in the Yaxcopoil-1 drilling as reported by Tuchscherer et al. (2004). The most evident difference is a slight shift of the samples of the sandstone complex towards the  $\text{FeO}+\text{MgO}$  corner, suggesting that the alteration of the glass involved a depletion of alkali elements which led to a relative enrichment in Fe and Mg; however, this relative enrichment is slightly misleading because it suggests a more basic precursor than it may have been in reality.

The low Al-normalized values of HFSE and LILE elements in the ejecta-rich lower part of the complex as compared to the upper part of the section and the opposite trend in the distribution of compatible elements (Fig. 4) suggest the involvement of some (possibly deeper seated), more basic crustal rocks with a similar trace-element pattern (Rudnick and Gao, 2003) in the composition of the melt that generated the spherules. In addition to the presence of amphibolites in outcrops of the basement lithologies of the Maya block along its southern margin and the occasional occurrence of altered mafic minerals and lithoclasts in drilling cores of the area (Donnelly et al., 1990; Kring et al., 2004), the contribution of mafic target components (diabase, pyroxenite, amphibolite) to the melt was suggested also by chemical and isotopic hints (Kring and Boynton, 1992; Kring et al., 1994; Kring et al., 2004; Ketrup et al., 2000). It is also conceivable that small amounts of mafic rocks from the lower crust were integrated into the impact melt. Based

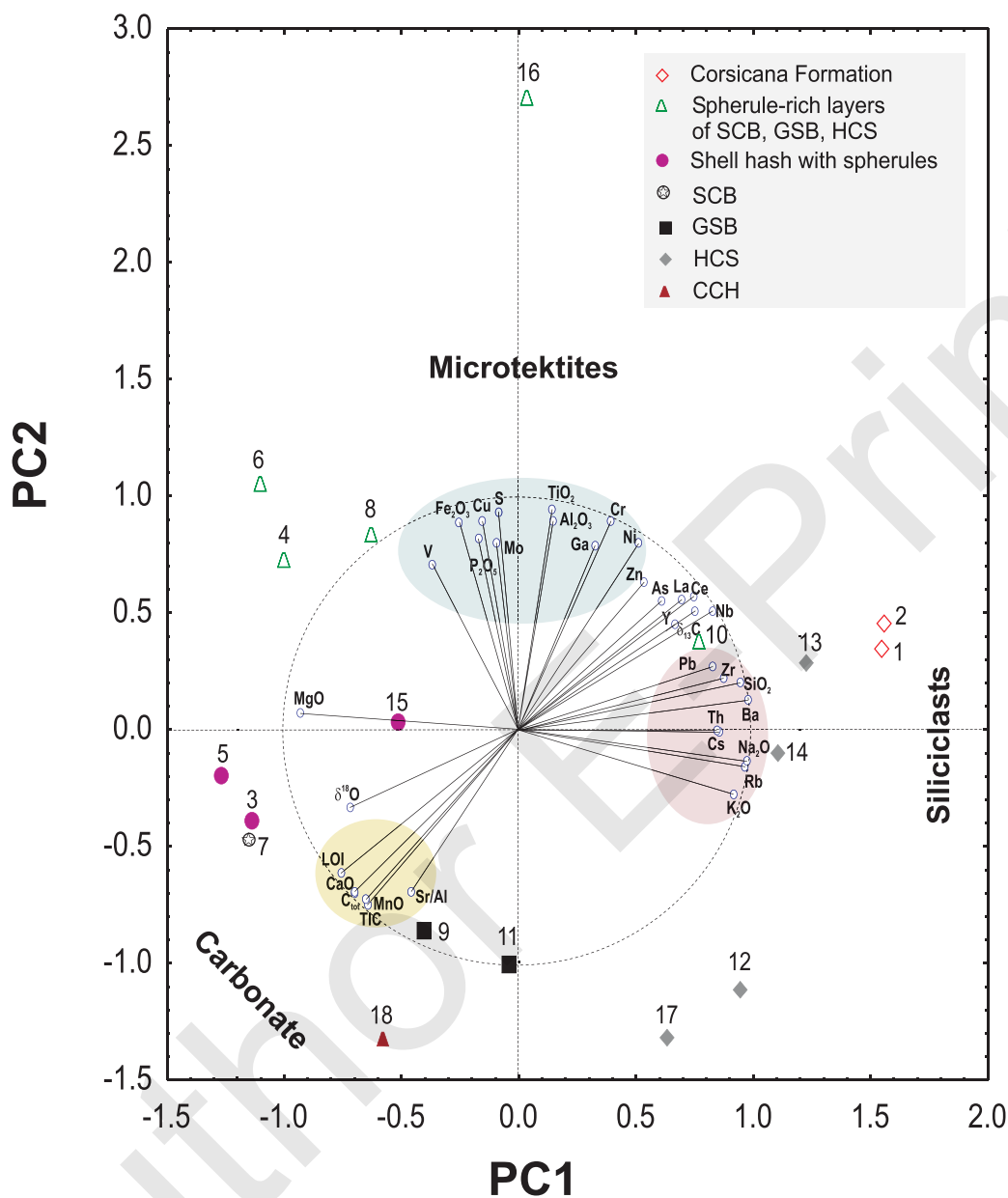


FIGURE 6.—Results of a principal-component analysis (PCA): vectors represent factor loadings and samples factor scores. PC1 corresponds to siliciclastic components, and PC2 corresponds to ejecta material, while the carbonate shows an opposite trend to both. Prior to PCA the major oxide contents were submitted to a centred logratio transformation in order to avoid closure effects.

on scaling calculations, Kring (1995) concludes that the impact excavated material from a depth of 12 to 14 km, while melting and displacement occurred down to a depth of 29 to 34 km. On the other hand, according to a standard profile of the continental crust (Wedepohl, 1995), the mafic granulites of the lower crust occur on average at a depth below ca. 32.8 km, which locally can be situated much higher.

The association of sulfur with PC2 and its relatively high contents in spherules is consistent with the presence of gypsum in the material composition of the ejecta (e.g., Heymann et al., 1998; Sigurdson et al. 1992; Bohor and Glass, 1995); together with the limestones, these formed the bulk of the deposits which covered the basement at the

impact site. Sulfur, which was initially dissolved in the glass, was evidently reduced to  $S^{2-}$  during alteration (or possibly later) by sulfate-reducing bacteria, thereby preventing the removal of chalcophile elements from the spherules, as supported by the association of PC2 with Fe, Cu, Ni, Mo, Zn, and As. The assimilation of Mn in the carbonate lattice (negative loadings in PC2) also indicates that the carbonate was deposited under reducing conditions.

Noteworthy is the presence of P together with S in the group of elements characteristic for the ejecta material. Certainly, the most straightforward explanation for the source of P is a sedimentary origin, as indicated by the presence of phosphorite clasts and phosphate of biogenic origin, as already shown by several previous authors (e.g.,

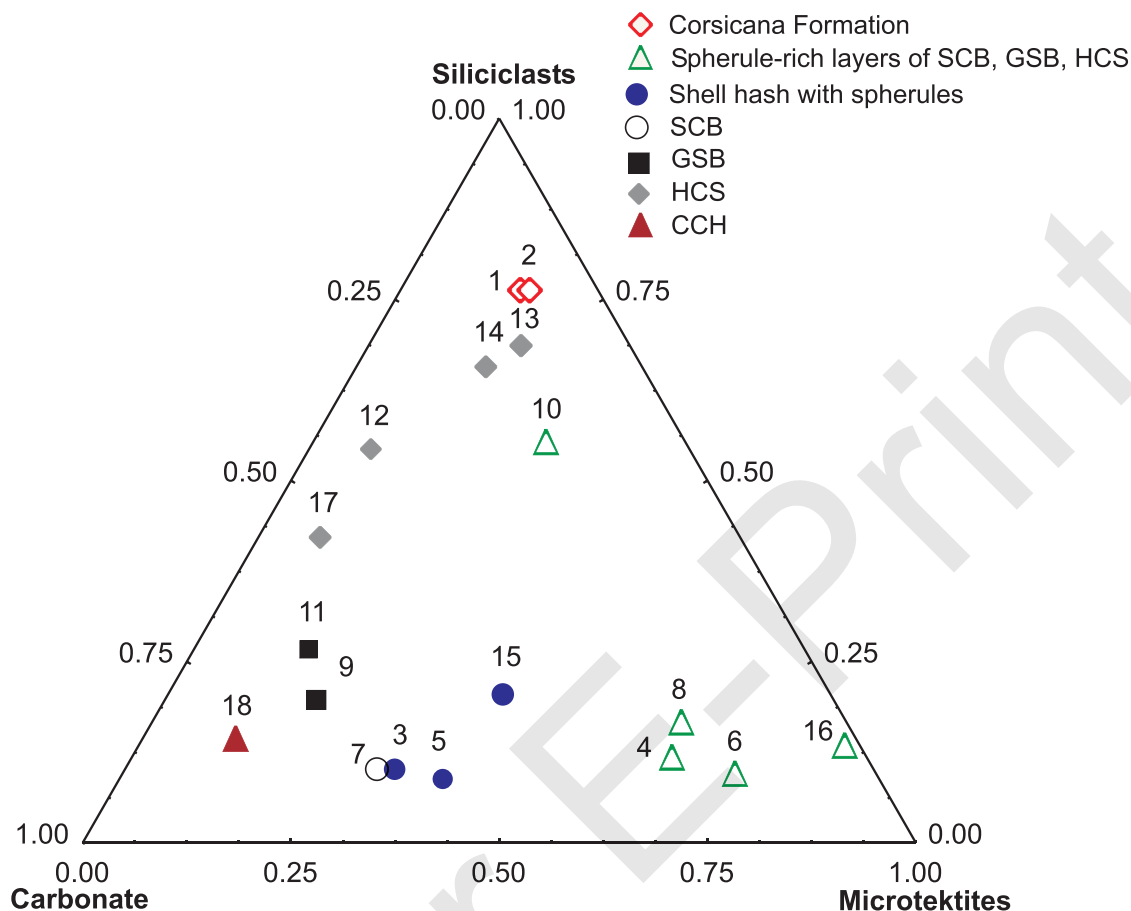


FIGURE 7.—Representation of the samples in a ternary diagram as a function of their major components by inverse mapping of the isometric logratio transformation (method after Ohta and Arai, 2007).

Schulte et al., 2006; Keller et al., 2007). However, the preferential association of P with the spherules, as clearly indicated by the present study, is very conspicuous and needs an explanation. Goyazite [ $\text{SrAl}_3(\text{PO}_4)_2(\text{OH})_5$ ]-bearing spherules were often reported in connection with altered KT microtektites and were interpreted to result from the interaction with phosphorus-rich diagenetic solutions percolating through the sediment (e.g., Pollastro and Pillmore, 1987; Smit et al., 1991; Bohor and Glass, 1995; Smit, 1999). However, it can be assumed that, similar to S, the high P content is a primary feature of the ejecta material and is due to phosphorite layers that occasionally may have been intercalated in the sedimentary sequence of the target area. The absence of phosphorite layers in a couple of discrete sampling sites (drillings) is certainly not a decisive rejecting argument, in that the sedimentologic setting of the target area is quite favorable for the formation of phosphorite deposits (e.g., Cook and Shergold, 2005). Smit et al. (1994) already suggested the presence of phosphorite deposits within the caprocks of the Chicxulub impact site based on Ca-phosphate grains observed in otherwise homogeneous Haitian tektite glass. There is no need to assume extended phosphorite deposits to explain the observed association: some thin layers intercalated in the stratigraphic sequence of the target deposits would be enough to yield slightly above-average P concentrations in parts of the deposited ejecta material. Although the presence of goyazite could not be demonstrated by XRD (probably due to its low contents) and consequently remains hypothetical, the strong correlation between Ca and the Al-normalized Sr contents, and the absence of a correlation between the bulk Sr and

Ca content (as would be generally expected), are indirect hints toward the presence of this secondary phosphate mineral. The assumption is supported also by a relatively good correlation between  $\text{Al}_2\text{O}_3$  and  $\text{P}_2\text{O}_5$  ( $r = 0.79$ ), a relationship otherwise unusual for calcite-bearing deposits. Phosphorus, together with excess Al and the Sr released during the alteration of biogenic aragonite to calcite (layers 3, 5, 15), may have participated in the formation of goyazite. Excess Mg not incorporated into smectite was taken up by secondary calcite, as suggested by the intermediate position (between the carbonate phase and altered spherule) of the vector representing the loading of the *clr* transformed Mg (Fig. 6).

The relationship between carbonate content and its isotope composition allows some constraints on the origin of carbonate in these deposits. A cross plot of the  $\delta^{13}\text{C}$  and  $\delta^{18}\text{O}$  values suggests three carbonate end members with distinct isotopic compositions: (1) Maastrichtian biogenic carbonate, (2) carbonate strongly depleted in  $^{13}\text{C}$ , and (3) carbonate depleted in  $^{18}\text{O}$  relative to the biogenic carbonate (Fig. 10). Carbonates in samples of the Corsicana Formation are evidently of biogenic origin, but those in the sandstone complex are a mixture of different proportions of these three end members. A more detailed study on the isotope composition of individual spherules (Ullrich et al., this volume) has shown that the low  $\delta^{13}\text{C}$  values are typical of the carbonate associated with spherules, while low  $\delta^{18}\text{O}$  values are found in spherule-like carbonate nodules (notably in layer 10), which according to Yancey and Guillemette (2008) represent accretionary lapilli formed within the ejecta plume from hot fluids. The

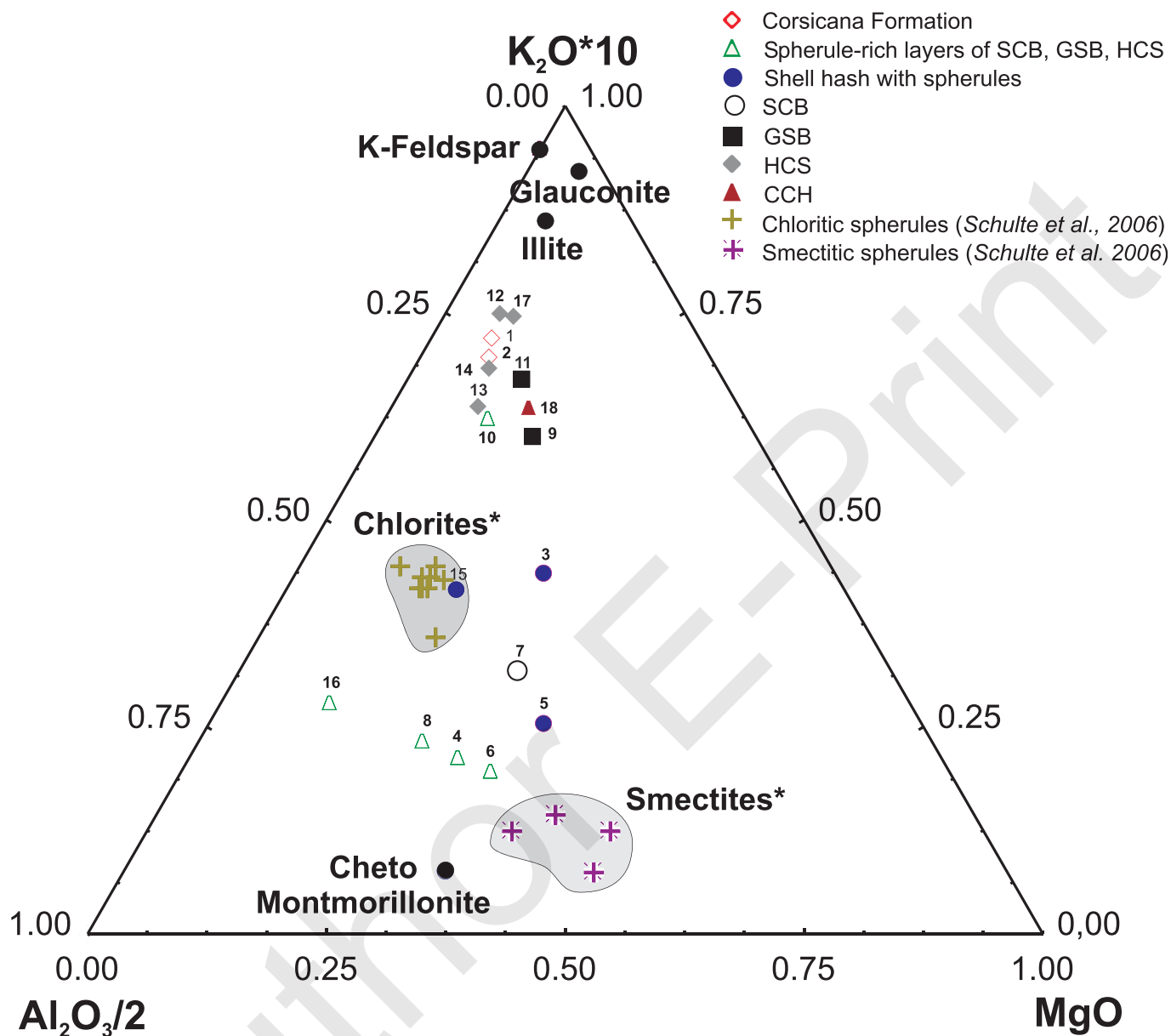


FIGURE 8.—Representation of the samples in a ternary diagram as a function of their  $\text{Al}_2\text{O}_3$ ,  $\text{MgO}$ , and  $\text{K}_2\text{O}$  content (note the distortion due to transformation of the  $\text{Al}_2\text{O}_3$  and  $\text{K}_2\text{O}$  values). Spherule-rich samples plot between the composition of smectite and chlorite spherules as reported in Schulte et al. (2006).

low  $\delta^{18}\text{O}$  values of these grains are consistent with high temperature during formation. In contrast, we interpret the low  $\delta^{13}\text{C}$  values of the carbonate associated with true spherules to be due to organic-rich intercalations in the target deposits, which were oxidized and reacted to Ca carbonate during the impact. A potential source for the  $^{13}\text{C}$ -depleted carbon in carbonate associated with the true spherules may be organic-rich layers in the target deposits, which were oxidized and reacted to Ca carbonate during or shortly after the impact. If so, a part of the carbonate associated with the spherules of the Brazos Riverbed section may have resulted not from diagenetic alteration but from segregation from a carbonate-rich silicate melt or formed by reaction of  $\text{CO}_2$ -rich gaseous inclusions with the hot CaO (supra)saturated silicate

melt. A more detailed discussion of this issue is presented by Ullrich et al. (this volume). The absence of carbonate infill in the tiny, alteration-prone spherules of layer 16 also suggests that it is unlikely that the  $^{13}\text{C}$ -depleted carbonate resulted from alteration of the spherules. The chemical index of alteration (CIA) calculated from carbonate subtracted analyses shows considerably lower values in the sandstone complex (40–70) than in the Corsicana Formation (around 80).

Their distinct isotope composition allows a rather accurate calculation of the relative portion of these three carbonate types in each of the layers (Fig. 11). While the lower part of the section (BCB and SCB) is dominated by a  $^{13}\text{C}$ -depleted carbonate typical of spherules, the HCS has a higher proportion of  $^{18}\text{O}$ -depleted carbonate

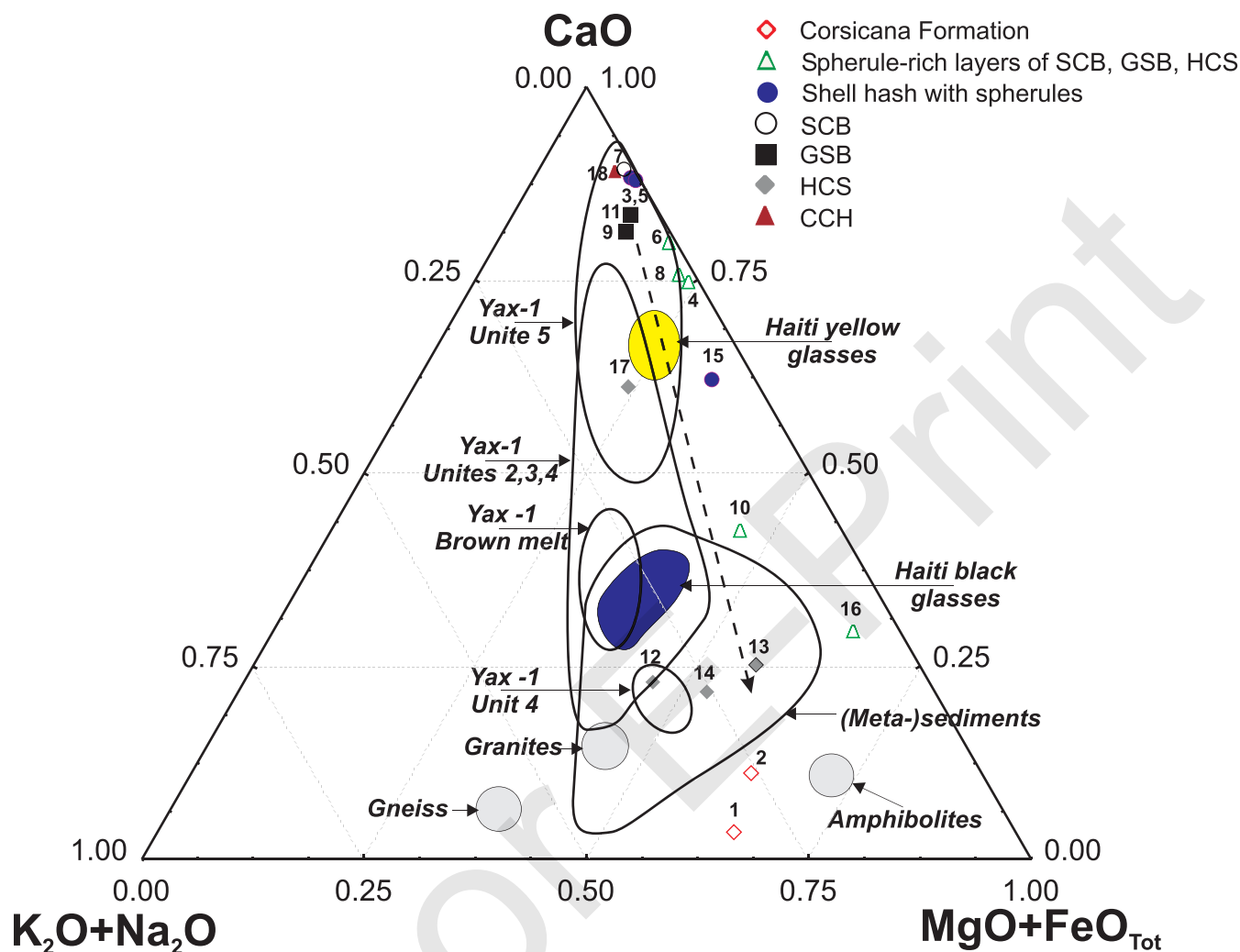


FIGURE 9.—Ternary  $K_2O+Na_2O-CaO-MgO+FeO_{Tot}$  plot showing the position of calcite-corrected bulk sample compositions in comparison with impactites recovered by the Yaxcopoil-1 drilling as reported by Tuchscherer et al. (2004). The general trend shown by the samples of the sandstone complex suggests a depletion in alkaline elements and a relative enrichment in Mg and Fe relative to the impactite lithological units of the Yaxcopoil-1 core. Units 1 to 3 are suevites; Unit 4 is a green impact melt breccia, and Unit 5 is a variegated, polymict, impact-melt breccia/suevite (Tuchscherer et al., 2004).

as characteristic of accretionary lapilli. Noteworthy exceptions include sample 16, which contains carbonaceous lapilli as well as tiny spherules that generally lack calcitic cores, and sample 10 of the GSB, in which the spherical grains are apparently represented chiefly by lapilli rather than by true spherules.

#### *Depositional Environment and Postdepositional Changes*

The transition from organic-rich claystones to a layer with spherule-bearing lithified claystone clasts at the base of the sandstone complex indicates the sudden switch to a high-energy hydraulic environment, which persisted through the deposition of the HCS. Considering the lateral discontinuity of these high-energy sediments, they most likely represent channel infills (Keller et al., 2007). The relative abundance of pyrite throughout the sandstone complex, notably in association with spherules, the accommodation of Mn in the lattice of the Ca carbonate, and the increase of the U/Th ratios and abundance of Mo in these

deposits suggest reducing conditions (e.g., Morford and Emmerson 1999; Mangini et al., 2001), which are rather unusual for a high-energy, commonly oxygen-rich environment. Sulfate released during alteration from glass was reduced to form pyrite, while P may have participated in formation of goyazite. Consequently, these aspects—including the alteration of the glass spherules into smectites and/or chlorite—must be secondary features that developed under reducing conditions, most likely in a shallow marine or inner-neritic environment. Because goyazite is considered to form preferentially in terrestrial environments (Smit et al., 1991; Hall et al., 1997), periodic subaerial exposure of the already deposited sediments is not unlikely and has been documented in the Mullinax-3 well to the south (Adate et al., this volume).

#### *Duration of Deposition*

Based primarily on sedimentological and biostratigraphic constraints, notably Keller and co-workers questioned the coincidence of

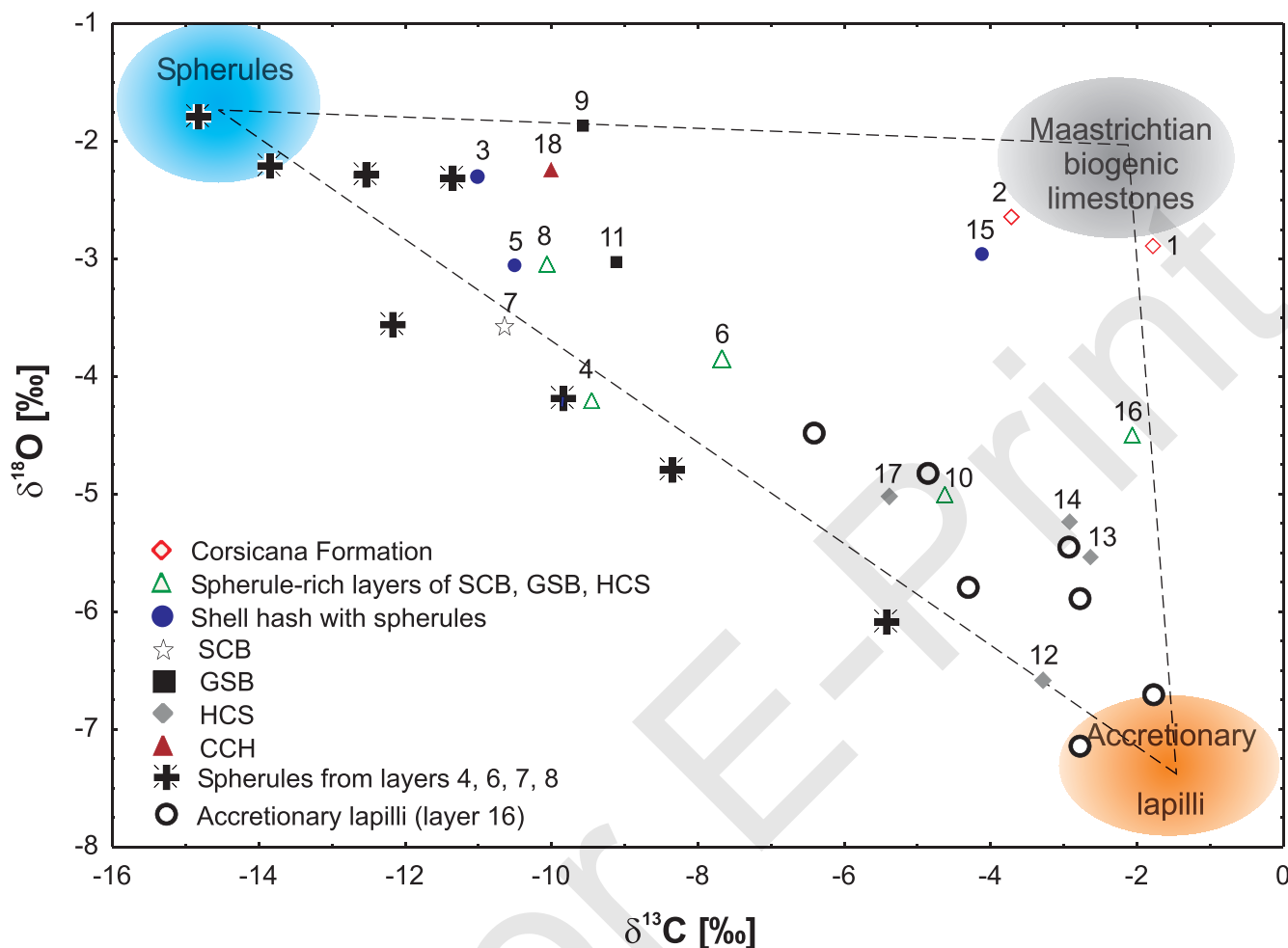


FIGURE 10.—The isotope compositions of carbonate in the samples represent a mixture between three end members: biogenic carbonate, carbonate associated with spherules and carbonate of the accretionary lapilli.

the Chicxulub impact and the KT extinction event (Keller et al., 1997; Keller et al., 2003; Keller et al., 2004a; Keller et al., 2004b; Keller et al., 2007; Keller et al., 2008; Keller et al., 2009). Their arguments are based primarily on the different stratigraphic positions of the biostratigraphically and isotopically defined KT boundary relative to the Chicxulub impact ejecta material (impact spherules and Ir anomalies), notably in the Caribbean, northeastern Mexico, and the Brazos area. Key to this argument is the time which elapsed from the first occurrence of impact markers to the mass extinction and the  $\delta^{13}\text{C}$  shift. If the Chicxulub impact predates the KT boundary, then it could not have been the primary cause of the mass extinction at the KT boundary.

The duration of sediment deposition is difficult to constrain on the basis of geochemical criteria alone, but the data presented here can be used to check the plausibility of the hypothesis that the sandstone complex was deposited from impact-generated tsunami waves within a short time interval (e.g., Bohor and Glass, 1995; Smit et al., 1996). This model generally assumes that, proximal to impact sites, the deposition of the fine, dispersed material of the vaporized bolide was preceded by the sedimentation of the coarse ejecta material that originated from the target rocks. If so, the portion of meteorite component, (i.e., the concentrations of elements of typical extraterrestrial origin) should be generally low in the spherule-bearing layers,

but should increase up-section within the sandstone complex. Except for two slightly increased Ir peaks of 1.1 and 0.2  $\mu\text{g}/\text{kg}$ , no further geochemical impact markers have been detected within the spherule-bearing deposits investigated here. Though relatively high, the concentration of Ir is still very low in chondrites (0.47 ppm; Henderson and Henderson, 2009), so that its accurate detection is practically not possible if the meteorite component is very low. In contrast, the huge difference with respect to both the concentrations and ratio of Ni to Cu in chondrites and in lithospheric crust (which are 10,640 ppm/ 127 ppm in C1 chondrite; 47 ppm/ 28 ppm, and 33.5 ppm /26 ppm in the upper and middle continental crust, respectively; Lodders, 2003; Rudnick and Gao, 2003) as well as their similar geochemical behavior during alteration, makes this element pair a potentially sensitive tracer for the amount of extraterrestrial material.

The increasing Ni/Cu ratios toward the top of the section (Fig. 12) is in agreement with a gradually increasing portion of meteorite component in the sediments, but this general trend is interrupted sharply in each layer of ejecta-rich material. Simple calculations show that the highest Ni/Cu ratios can be explained by the addition of less than 1% of chondritic material. The breaks in the trend, however, seem to disprove deposition of the material within a single event, which would imply a continuously increasing portion of sub-micrometer chondritic dust settled out from the fireball cloud (e.g., Bohor and

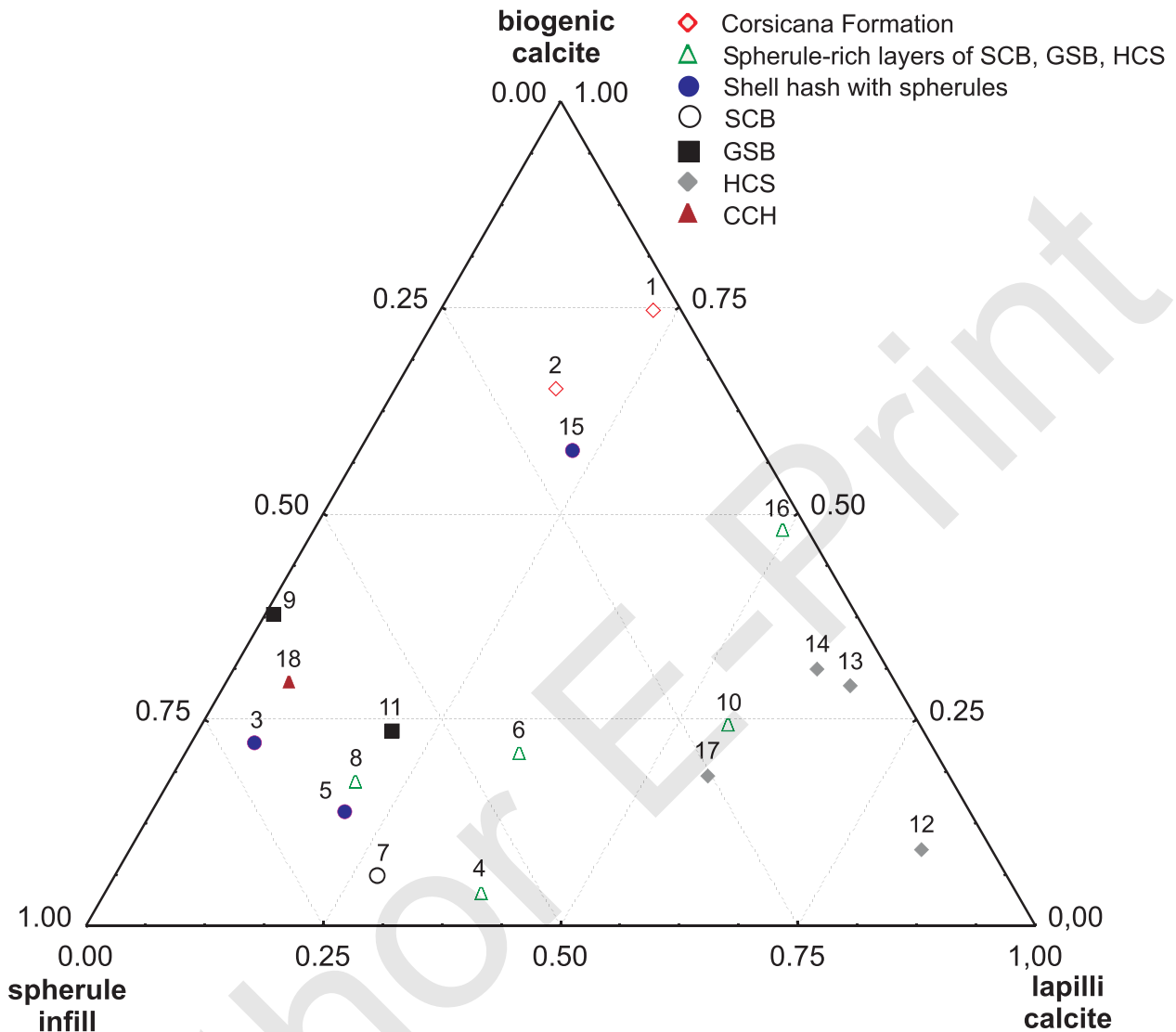


FIGURE 11.—Relative portions of biogenic calcite ( $\delta^{13}\text{C} = -1.5\text{‰}$ ;  $\delta^{18}\text{O} = -1.0\text{‰}$ ), of calcite typical of accretionary lapilli ( $\delta^{13}\text{C} = -1.5\text{‰}$ ;  $\delta^{18}\text{O} = -7.5\text{‰}$ ) and of calcite that forms the cores of spherules with a clayey outer shell ( $\delta^{13}\text{C} = -15.0\text{‰}$ ;  $\delta^{18}\text{O} = -2.0\text{‰}$ ). The relative amounts were calculated by assigning the  $\delta$  values (in brackets) to the end members.

Glass, 1995; Kyte and Bostwick, 1995; Smit, 1999). The observed pattern is more likely due to the addition of different portions of clastic components to the sediment, as supported by a good correlation ( $r = 0.82$ ) between the Ni/Cu ratio and the amount of siliciclastic components, as assessed from the *ilr* transformed factor scores. The higher Ni/Cu ratios in the Corsicana Formation (2.0–2.2) relative to the middle/upper crust (1.29 and 1.67, respectively) are also in line with this interpretation. A similar trend can be deduced also from the Ti/Cr ratio, an element pair which also shows contrasting abundances in meteorites and as compared to crustal rocks (Rudnick and Gao, 2003).

Although Ir contents in the sandstone complex of the Brazos area are generally low, except for occasional, transient peaks, it is noteworthy that high Ir concentrations occur consistently in an interval immediately above and bracketed between the HCS (if present) and the biostratigraphically defined KT boundary (see figures in Gertsch et al., this volume). The persistence of increased Ir contents distributed throughout several tens of centimeters must be explained if it is

assumed that deposition occurred over a considerable time interval. The roughly flat chondrite-normalized pattern of the PGEs indicates a dominantly cosmic source and would imply an increased cosmic PGE input over time scales of tens of thousands of years. In our opinion, a substantial postdepositional remobilization, let alone a concentration of the PGEs by redox processes, without a dramatic change in the chondritic pattern, is not justified. Reworking of older sediments with high Ir contents, increased input of cosmic dust, or low sedimentation rates over the time interval considered (Bruns et al., 1997) are conceivable causes which may explain the observed distribution of Ir concentrations over several tens of centimeters below the actual KT boundary.

## CONCLUSIONS

The lithologies of the sandstone complex in the Brazos Riverbed section are a mixture of different proportions of clastic compounds,

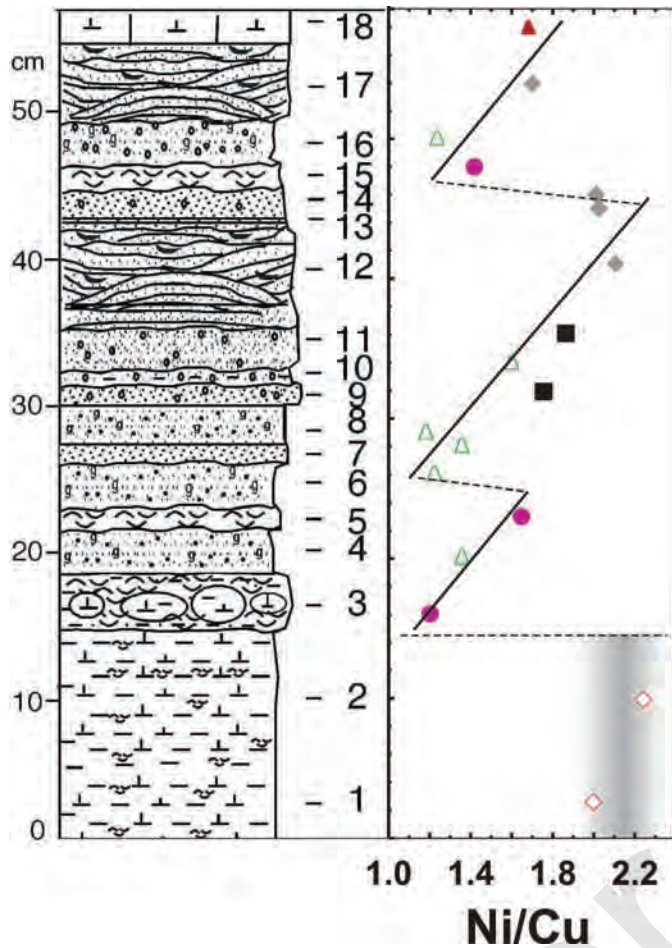


FIGURE 12.—Variation of the Ni/Cu ratio along the section as an expression of the portion of chondritic material in the samples (see explanations in text).

ejecta material, and calcite. The microtektites represent glass spherules altered completely to clay minerals (dominantly smectite and subordinately chlorite). The isotopic composition of the calcite in the sediments indicates three kinds of carbonates of different origin: biogenic calcite, calcite in the core of spherules, and calcite associated with accretionary lapilli. Differences in the abundances of major elements and trace elements in the spherule-rich and spherule-barren layers suggest that the source of the microtektites are rocks of the upper and/or middle continental crust mixed with sediments that covered the basement at the impact site. High S and P contents in the most spherule-rich layers and the unusually low  $\delta^{13}\text{C}$  value of the associated carbonate (limestones and evaporites) suggest a more complex lithology in the target area, which may also have included phosphorites and organic-rich layers. Except for the spherules and a moderately high Ir peak, no further impact markers were detected in the studied section. Variations in the Ni/Cu ratio, used to trace the portion of the meteoritic component in the sediment, do not support a model according to which the sandstone complex was deposited in a short interval of time in the wake of a single impact event. Also, the inconsistency between features that indicate a prevalence of reducing conditions during the alteration of the ejecta material (pyrite inclusions in spherules, accommodation of  $\text{Mn}^{2+}$  by secondary calcite) and sedimentologic features which point toward the deposition of the sandstone complex in a dominantly oxic,

high-energy environment, strongly support the case that the ejecta material in these deposits was reworked.

## ACKNOWLEDGMENTS

This study was carried out within a project funded by the Deutsche Forschungsgemeinschaft (Stu 169/34). We thank the reviewers, R. Martinez-Ruiz and one anonymous, for their thoughtful comments and suggestions. G. Keller is acknowledged for her valuable comments and support in the field work. The authors thank U. Kramar, B. Oetzel (ED-/WD-XRF, XRD), C. Haug (Ni-fire assay), C. Mössner (HR-ICP-MS), and G. Preuss (IRMS) for their support in the manifold analytical work. L. Fay is acknowledged for her help in editing this manuscript.

## REFERENCES

- ADATTE, T., STINNESBECK, W., AND KELLER, G., 1996, Lithostratigraphic and mineralogical correlations of near K-T boundary clastic sediments in northeastern Mexico: Implications for mega-tsunami or sea level changes?, *in* Ryder, G., Fastovsky, D., and Gartner, S., eds., *The Cretaceous-Tertiary Event and Other Catastrophes in Earth History: Geological Society of America, Special Paper 307*, p. 197–210.
- ARENILLAS, I., ARZ, J.A., GRAJALES-NISHIMURA, J.M., MURILLO-MUNETON, G., ALVAREZ, W., CAMARGO-ZANOQUERA, A., MOLINA, E., AND ROSALES-DOMINGUEZ, C., 2006, Chicxulub impact event is Cretaceous/Paleogene boundary in age: New micropaleontological evidence: *Earth and Planetary Science Letters*, v. 249, p. 241–257.
- BOHOR, B.F., AND GLASS, B.P., 1995, Origin and diagenesis of K/T impact spherules—from Haiti to Wyoming and beyond: *Meteoritics*, v. 30, p.182–198.
- BOURGEOIS, J., HANSEN, T.A., WIBERG, P., AND KAUFFMAN, E.G., 1988, A tsunami deposit at the Cretaceous-Tertiary boundary in Texas: *Science*, v. 141, p. 567–570.
- BRUNS, P., RAKOCZY, H., PERNICKA, E., AND DULLO, W.-C., 1997, Slow sedimentation and Ir anomalies at the Cretaceous/Tertiary boundary: *Geologische Rundschau*, v. 86, p.168–177.
- COOK, P.J., AND SHERGOLD, J.H., EDS., 2005, *Phosphate deposits of the World. Vol. 1—Proterozoic and Cambrian Phosphorites*: Cambridge, U.K., Cambridge University Press, p. 408.
- DRESSLER, B.O., SHARPTON, V.L., SCHWANDT, C.S., AND AMES, D., 2004, Impactites of the Yacopoil-1 drilling site, Chicxulub impact structure: Petrography, geochemistry, and depositional environment: *Meteoritics & Planetary Science*, v. 39, p. 857–878.
- DONNELLY, T.W., HORNE, G.S., FINCH, R.C., AND LÓPEZ-RAMOS, E., 1990, Northern Central America; The Maya and Chortis blocks, *in* Dengo, G., and Case, J.E., eds., *The Geology of North America, Vol. H—The Caribbean Region*: Boulder, Geological Society of America, p. 37–76.
- EKDALE, A.A., AND STINNESBECK, W., 1998, Trace fossils in Cretaceous-Tertiary (KT) boundary beds in northeastern Mexico: Implications for sedimentation during the KT boundary event: *Palaios*, v.13, p. 593–602.
- GALE, A.S., 2006, The Cretaceous-Paleogene boundary on the Brazos River, Falls County, Texas: Is there evidence for impact-induced tsunami sedimentation?: *Proceedings of the Geologists' Association*, v. 117, p. 173–185.
- HALL, R.B., FOORD, E.E., KELLER, D.J., AND KELLER, W.D., 1997, Phosphates in some Missouri refractory clays: *Clays and Clay Minerals*, v. 45, p. 353–364.
- HANSEN, T., FARRAND, R.B., MONTGOMERY, H.A., BILLMAN, H.G., AND BLECHSCHMIDT, G., 1987, Sedimentology and extinction patterns across the Cretaceous-Tertiary boundary interval in East Texas: *Cretaceous Research*, v. 8, p. 229–252.
- HENDERSON, P., AND HENDERSON, G.M., 2009, *The Cambridge Handbook of Earth Science Data*: Cambridge, U.K., Cambridge University Press, p. 277.
- HEYMANN, D., YANCEY, T.E., WOLBACH, W.S., THIEMENS, M.H., JOHNSON, E.A., ROACH, D., AND MOECKER, S., 1998, Geochemical markers of the Cretaceous-Tertiary boundary event at Brazos River, Texas, USA: *Geochimica et Cosmochimica Acta*, v. 62, p. 173–181.
- KELLER, G., LOPEZ-OLIVA, J.G., STINNESBECK, W., AND ADATTE, T., 1997, Age, stratigraphy and deposition of near-K/T siliciclastic deposits in Mexico:

- Relation to Bolide Impact?: Geological Society of America, Bulletin, v. 109, p. 410–428.
- KELLER, G., STINNESBECK, W., ADATTE, T., AND STÜBEN, D., 2003, Multiple impacts across the Cretaceous–Tertiary boundary: Earth-Science Reviews, v. 62, p. 327–363.
- KELLER, G., ADATTE, T., STINNESBECK, W., REBOLLEDO-VIEYRA M., URRUTIA FUCUGAUCHI, J., KRAMAR, G., AND STUEBEN, D., 2004a, Chicxulub predates the K/T boundary mass extinction: National Academy of Sciences (USA), Proceedings, v. 101, p. 3753–3758.
- KELLER, G., ADATTE, T., STINNESBECK, W., STUEBEN, D., BERNER, Z., KRAMAR, U., AND HARTING, M., 2004b, More evidence that the Chicxulub impact predates the K/T Mass Extinction: Meteoritics & Planetary Science, v. 39, p. 1127–1144.
- KELLER, G., ADATTE, T., BERNER, Z., HARTING, M., BAUM, G., PRAUSS, M., TANTAWY, A., AND STÜBEN, D., 2007, Chicxulub impact predates K–T boundary: New evidence from Brazos, Texas: Earth and Planetary Science Letters, v. 255, p. 339–356.
- KELLER, G., ADATTE, T., BAUM, G., AND BERNER, Z., 2008, Reply to ‘Chicxulub impact predates K–T boundary: New evidence from Brazos, Texas’. Comment by Schulte et al.: Earth and Planetary Science Letters, v. 269, p. 620–628.
- KELLER, G., ADATTE, T., PARDO, A., AND LOPEZ-OLIVA, L., 2009, Age and biotic effects of the Chicxulub impact in Mexico: Geological Society of London, Journal, v. 166, p. 393–411.
- KETTRUR, B., DEUTSCH, A., OSTERMANN, M., AND AGRINIER, P., 2000, Chicxulub impactites: Geochemical clues to the precursor rocks: Meteoritics & Planetary Science, v. 35, p. 1229–1238.
- KRING, D.A., 1995, The dimensions of the Chicxulub impact crater and impact melt sheet: Journal of Geophysical Research, v. 100, p. 16,979–16,986.
- KRING, D.A., AND BOYNTON, W.V., 1992, The petrogenesis of an augite-bearing melt rock in the Chicxulub structure and its relationship to K/T impact spherules in Haiti: Nature, v. 358, p. 141–144.
- KRING, D.A., HILDEBRAND, A.R., AND BOYNTON, W.V., 1994, Provenance of mineral phases in the Cretaceous–Tertiary boundary sediments exposed on the southern peninsula of Haiti: Earth & Planetary Science Letters, v. 128, p. 629–641.
- KRING, D.A., HÖRZ, H., ZURCHER, L., AND URRUTIA FUCUGAUCHI, J., 2004, Impact lithologies and their emplacement in the Chicxulub impact crater: Initial results from the Chicxulub Scientific Drilling Project, Yaxcopoil, Mexico: Meteoritics & Planetary Science, v. 39, p. 879–897.
- KYTE, F.T., AND BOSTWICK, J.A., 1995, Magnesioferrite spinel in Cretaceous/Tertiary boundary sediments of the Pacific basin: remnants of hot, early ejecta from the Chicxulub impact?: Earth and Planetary Science Letters, v. 132, p. 113–27.
- LODDERS, K., 2003, Solar system abundances and condensation temperatures of the elements: The Astrophysical Journal, v. 591, p. 1220–1247.
- MANGINI, A., JUNG, M., AND LAUKENMANN, S., 2001, What do we learn from peaks of uranium and of manganese in deep sea sediments?: Marine Geology, v. 177, p. 63–78.
- MORFORD, J.L., AND EMERSON, S.R., 1999, The geochemistry of redox sensitive trace metals in sediments: Geochimica et Cosmochimica Acta, v. 63, p. 1735–1750.
- OHTA, T., AND ARAI, H., 2007, Statistical empirical index of chemical weathering in igneous rocks: A new tool for evaluating the degree of weathering: Chemical Geology, v. 240, p. 280–297.
- POLLASTRO, R.M., AND PILLMORE, C.L., 1987, Mineralogy and petrology of the Cretaceous–Tertiary boundary clay bed and adjacent clay-rich rocks, Raton basin, New Mexico and Colorado: Journal of Sedimentary Petrology, v. 57, p. 456–466.
- RUDNICK, R.L., AND GAO, S., 2003, Composition of the continental crust, in Holland, E.D., and Turekian, K.K., eds., Treatise on Geochemistry, v. 3, Rudnick, R.L.: The Crust: Oxford, U.K., Elsevier-Pergamon, p. 659.
- SCHMITT, R.T., WITTMANN, A., AND STÖFFLER, D., 2004, Geochemistry of drill core samples from Yaxcopoil-1, Chicxulub impact crater, Mexico: Meteoritics & Planetary Science, v. 39, p. 979–1001.
- SCHULTE, P., STINNESBECK, W., STÜBEN, D., KRAMAR, U., BERNER, Z., KELLER, G., AND ADATTE, T., 2003, Fe-rich and K-rich mafic spherules from slumped and channelized Chicxulub ejecta deposits in the northern La Sierrita area, NE Mexico: International Journal of Earth Sciences (Geologische Rundschau), v. 92, p. 114–142.
- SCHULTE, P., SPEIJER, R., MAI, H., AND KONTNY, A., 2006, The Cretaceous–Paleogene (K–P) boundary at Brazos, Texas: Sequence stratigraphy, depositional events and the Chicxulub impact: Sedimentary Geology, v. 184, p. 77–109.
- SIGURDSSON, H., D’HONDT, S., AND CAREY, S., 1992, The impact of the Cretaceous/Tertiary bolide on evaporite terrane and generation of major sulfuric acid aerosol: Earth and Planetary Science Letters, v. 109, p. 543–559.
- SMIT, J., 1999, The global stratigraphy of the Cretaceous–Tertiary boundary impact ejecta: Annual Review of Earth and Planetary Sciences, v. 27, p. 75–113.
- SMIT, J., VAN EIJDEN, A.J.M., AND TROELSTRA, S.R., 1991, Analysis of the Australasian microtektite event, the Toba Lake event, and the Cretaceous/Paleogene boundary, Eastern Indian Ocean, in Weissel, J., Peirce, J., Taylor, E., Alt, J., et al., eds., Proceedings of the Ocean Drilling Program, Scientific Results, v. 121. College Station, TX, p. 489–503, doi:10.2973/odp.proc.sr.121.149.1991
- SMIT, J., MONTANARI, A., SWINBURNE, N.H.M., ALVAREZ, W., HILDEBRAND, A.R., MARGOLIS, S.V., CLAEYS, P., LOWRIE, W., AND ASARÓ, F., 1992, Tektite-bearing, deep-water clastic unit at the Cretaceous–Tertiary Boundary in northeastern Mexico: Geology, v. 20, p. 99–103.
- SMIT, J., BEETSMA, J.J., VONHOF, H.B., PRINGLE, M.J., AND WIJBRANS, J.R., 1994, Geochemistry and Sr, Nd, Ar isotope systematics of Haitian K/T tektites and Chicxulub impact melt (abstract), in Lanphere, M.A., Dalrymple, G.B., and Turrin, B.D., eds., Abstracts of the Eighth International Conference on Geochronology, Cosmochronology and Isotope Geology, Berkeley, California, USA, June 5–11, 1994: US Geological Survey, Circular 1107, p. 295.
- SMIT, J., ROER, T.B., ALVAREZ, W., MONTANARI, A., CLAEYS, P., GRAJALES-NISHIMURA, J.M., AND BERMUDEZ, J., 1996, Coarse-grained, clastic sandstone complex at the K/T boundary around the Gulf of Mexico: Deposition by tsunami waves induced by the Chicxulub impact? in Ryder, G., Fastovsky, D.E., and Gartner, S., eds., The Cretaceous–Tertiary Event and Other Catastrophes in Earth History: Geological Society of America, Special Paper 307, p. 151–182.
- STINNESBECK, W., BARBARIN, J.M., KELLER, G., LOPEZ-OLIVA, J.G., PIVNIK, D.A., LYONS, J.B., OFFICER, C.B., ADATTE, T., GRAUP, G., ROCCHIA, R., AND ROBIN, E., 1993, Deposition of channel deposits near the Cretaceous–Tertiary boundary in northeastern Mexico: Catastrophic or “normal” sedimentary deposits?: Geology, v. 21, p. 797–800.
- TUCHSCHERER, M.G., REIMOLD, W.U., KOEBERL, CH., AND GIBSON, R.L., 2004, Major and trace element characteristics of impactites from the Yaxcopoil-1 borehole, Chicxulub structure, Mexico: Meteoritics & Planetary Science, v. 39, p. 955–978.
- WEDEPOHL, K.H., 1995, The composition of the continental crust: Geochimica et Cosmochimica Acta, v. 59, p. 1217–1232.
- YANCEY, T.E., 1996, Stratigraphy and depositional environment of the Cretaceous–Tertiary boundary complex and basal Paleocene section, Brazos River, Texas: Gulf Coast Association of Geological Societies, Transactions, v. 64, p. 433–442.
- YANCEY, T.E., AND GUILLETTE, R.N., 2008, Carbonate accretionary lapilli in distal deposits of the Chicxulub impact event: Geological Society of America, Bulletin, v. 120, p. 1105–1118.